Continental Shelf Research 31 (2011) 433–447

Contents lists available at ScienceDirect

Continental Shelf Research

journal homepage: www.elsevier.com/locate/csr

Onshore–offshore gradient in reductive early diagenesis in coastal marine sediments of the Ria de Vigo, Northwest Iberian Peninsula

K.J. Mohamed [a,*,1], D. Rey [a], B. Rubio [a], M.J. Dekkers [b], A.P. Roberts [c,2], F. Vilas [a]

[a] Depto. de Geociencias Marinas y Ordenación del Territorio, Universidad de Vigo, Lagoas-Marcosende S/N, Vigo, 36310, Spain
[b] Paleomagnetic Laboratory 'Fort Hoofddijk', Department of Earth Sciences, Utrecht University, Budapestlaan 17, 3584 CD, Utrecht, The Netherlands
[c] School of Ocean and Earth Science, National Oceanography Centre, University of Southampton, European Way, Southampton, SO14 3ZH, UK

ARTICLE INFO

Article history:
Received 8 January 2010
Received in revised form
27 May 2010
Accepted 1 June 2010
Available online 11 June 2010

Keywords:
Early diagenesis
Magnetic minerals
Reductive dissolution
Greigite
Coastal sediments
$CaCO_3$-related proxies

ABSTRACT

Early diagenetic modification of magnetic properties is an important process in marine sediments, but temporal and spatial variability of diagenetic processes have rarely been reported for recent coastal sediments. The magnetic properties of sediments from the Ria de Vigo (NW Spain) define a marked three-part zonation with depth. The uppermost zone is magnetically dominated by (titano-)magnetite. In the intermediate zone, rapid down-core dissolution of (titano-)magnetite increases the relative influence of high-coercivity magnetic minerals, which react more slowly during reductive dissolution than (titano-)magnetite. This zone is characterized by the ubiquitous occurrence of framboidal iron sulphides. Pyrite is the dominant iron sulphide, but framboidal ferrimagnetic greigite is also frequently observed in association with pyrite. The lowermost zone is characterized by an almost complete depletion of magnetic minerals associated with progressive reduction of detrital iron oxides with depth. This zonation is controlled by organic matter diagenesis, which varies with water depth and wave-induced sediment resuspension and organic matter reoxidation in the water column. This leads to a shallowing and thinning of each zone with more intense reductive diagenesis toward the interior of the ria. Such a zonation seems to be a common feature in shallow water marine environments. If preserved, the described zonation and its spatial variability provide a potential tool for detecting estuarine-like environments in the geological record. Magnetic detection of current or past reductive conditions also has important implications for assessing paleoenvironmental proxies that are sensitive to diagenetic redox state.

1. Introduction

Magnetic properties have proven to be useful in a wide range of paleoenvironmental applications in marine sediments (e.g. Robinson, 1986; Bloemendal et al., 1988; Bloemendal and deMenocal, 1989; Moreno et al., 2002; Snowball and Moros, 2003; Rousse et al., 2006). Magnetic properties are also highly sensitive to the redox state of the sediment, with suboxic conditions giving rise to alteration or even complete dissolution of magnetic iron oxides (Froelich et al., 1979), which complicates paleoenvironmental interpretations. As such, these diagenetically controlled alterations of magnetic minerals can be used to obtain paleoenvironmental information, such as reconstructions of variations in bottom water ventilation of marine basins (Larrasoaña et al., 2003).

Suboxic sediments typically exhibit large decreases in magnetization and changes in magnetic mineralogy and magnetic mineral grain size, which are associated with magnetite dissolution and pyrite formation as sulphate reduction proceeds (e.g. Karlin and Levi, 1983; Karlin, 1990; Bloemendal et al., 1992; Robinson et al., 2000; Robinson and Sahota, 2000; Rey et al., 2005, 2008). During pyritization, ferrimagnetic intermediate sulphides such as greigite can form and be preserved (Roberts and Turner, 1993; Horng et al., 1998; Kao et al., 2004; Roberts and Weaver, 2005; Larrasoaña et al., 2007). Greigite is ferrimagnetic and thus able to carry a remanent magnetization, and if pyritization is arrested before completion it can have important implications for the paleomagnetic (Jiang et al., 2001; Sagnotti et al., 2005; Roberts and Weaver, 2005; Rowan et al., 2009) and paleoceanographic record (Strechie et al., 2002; Larrasoaña et al., 2007; Blanchet et al., 2009; Zheng et al., 2010).

Despite the implications of early diagenesis on the marine sedimentary record, only a few studies have focused on the

* Corresponding author. Tel.: +34 986 812637; fax: +34 986 812556.
E-mail address: kmohamed@uvigo.es (K.J. Mohamed).
[1] Present address: Dept. of Geology and Geophysics, Woods Hole Oceanographic Institution, 266 Woods Hole Rd, Woods Hole, MA, 02543, USA.
[2] Now at: Research School of Earth Sciences, The Australian National University, Canberra, ACT 0200, Australia.

0278-4343/$ - see front matter © 2010 Elsevier Ltd. All rights reserved.
doi:10.1016/j.csr.2010.06.006

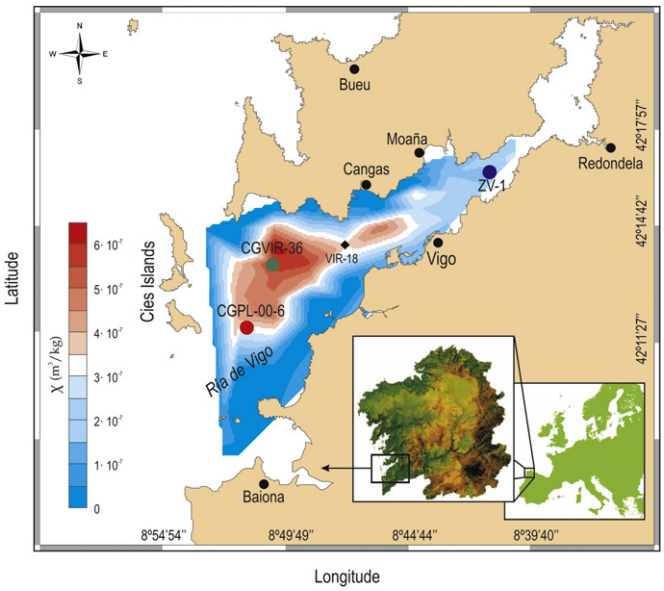

Fig. 1. Location of the cores studied in the Ria de Vigo (NW Iberian Peninsula). The coloured contour map represents the magnetic susceptibility of the surficial sediments (Rey et al., 2000). Core VIR-18 (diamond), dated by Diz et al. (2002), is also shown.

high-resolution characterization of diagenetic processes in recent coastal sediments (Emiroğlu et al., 2004; Liu et al., 2004) along with its spatial variability (Rey et al., 2005). These processes have a clear societal relevance. For example, the mobility of trace and rare earth elements in sediments, which may be deposited in urban settings, is controlled by the redox state of shallow sediments (e.g. Álvarez-Iglesias and Rubio, 2008, 2009; Caetano et al., 2009). Also, interpretation of proxies that are sensitive to changes in pore water chemistry driven by early diagenesis, such as the elemental and isotopic composition of $CaCO_3$ (McCorkle et al., 1995; Hover et al., 2001; Rudnicki et al., 2001; Regenberg et al., 2006), may be compromised unless the extent of early diagenesis is known.

The Ria de Vigo in the NW Iberian Peninsula (Fig. 1) is particularly well suited for analyzing ongoing magnetic mineral changes driven by early diagenesis. Biological productivity is enhanced by seasonal coastal upwelling from May to September (Fraga, 1981) and by intensive mussel farming from floating rafts. In addition, the interaction of wave climate and the physiography of the ria, which control sediment resuspension, leads to well defined sedimentological, geochemical and magnetic gradients in the surficial sediments (Rey et al., 2000; Vilas et al., 2005), which can explain observed spatial differences in diagenetic evolution with depth. We demonstrate in this paper how variations in these biological, physical and chemical processes influence reductive sedimentary diagenesis in a coastal marine environment.

2. Regional setting and sampling

The Ria de Vigo (Fig. 1) is the southernmost of four adjacent valleys or rias that are collectively known as the Rias Baixas, which were flooded during the sea-level rise after the last glacial maximum. In the Ria de Vigo, water depths range from 7 m in the inner part to 50 m at its mouth. The Cies Islands partially enclose the ria, and reduce the impact of south-westerly winter storms. This protection, along with the physiography of the ria, influences the wave energy distribution, which has an important control on the distribution of surficial sediments (Vilas et al., 2005). High energy areas in the ria margins are dominated by coarse sediments, while finer organic-rich sediments accumulate along the deep central axis and in the more quiet inner ria. The magnetic susceptibility of surficial sediments (Fig. 1) has a pattern that is controlled by mud and organic carbon contents. Higher magnetic susceptibilities are associated with muddy, low organic carbon content sediments that are typical of the outer ria central axis (Rey et al., 2000).

Primary production in the Ria de Vigo averages 292 gC m^{-2} yr^{-1} (Prego, 1993) and is driven by the Iberian upwelling. Based on a 30% export efficiency to the sediment and a 90% remineralization of this exported carbon (Wollast, 1998), the sediments of the Ria de Vigo incorporate ~9 gC m^{-2} yr^{-1}. Subsequent microbially mediated organic carbon oxidation therefore leads to depletion of dissolved oxygen in pore waters with depth and the onset of reductive diagenetic conditions.

3. Methods

The three gravity cores analyzed in this study (Fig. 1) were collected between 1999 and 2001 from the central axis of the Ria de Vigo in the outer (CGPL-00-6, 42°11′36″N, 8°51′25″W, 402 cm long, 40 m water depth), middle (CGVIR-36, 42°13′32″N, 8°50′20″W, 81 cm long, 39 m water depth) and inner (ZV-1, 42°16′25″N, 8°41′13″W, 249 cm long, 20 m water depth) ria sectors. The cores were located along a transect with mud contents >90% and increasing organic matter content and reducing conditions from the outer to the inner ria (Rey et al., 2000; Vilas et al., 2005). The cores were stored for less than two weeks at 4 °C. After storage the cores were split in half along their axes, described and X-ray radiographed using a Faxitron X-ray cabinet HP 43805 N. Colour descriptions are based on the Munsell Soil Colour Table (Munsell Color Company, 1994). Sampling was performed after core description using plastic cylinder containers of standard paleomagnetic size (2.5 cm diameter, 2.2 cm high) at stratigraphic intervals of 3 cm in cores CGVIR-36 and CGPL-00-6 and 2.5 cm for the upper 60 cm of core ZV-1. Below this depth the sampling interval was increased to 5 cm in core ZV-1 based on an expected lower variability of magnetic properties due to increased diagenetic reduction with depth.

Age control for core CGPL-00-6 is based on two multispecific foraminifera AMS ^{14}C dates. The Calib 5.0 program (Stuiver and Reimer, 1993) and the Marine Calibration Dataset Marine04 (Hughen et al., 2004) were used to calibrate radiocarbon dates to calendar years BP (cal yr BP). A local reservoir difference of -7 ± 90 yr (Soares, 1993) was included for samples younger than 1100 ^{14}C yr BP. The age model for core ZV-1 was developed from a palynological record by Muñoz Sobrino et al. (2007). Sedimentation rates for core CGVIR-36 are estimated from published chronologies for core VIR-18 (Diz et al., 2002; Desprat et al., 2003), which is also located in the middle sector of the ria (Fig. 1).

Grain size measurements for the >63 μm sediment fraction were performed using dry sieving. The mud fraction (<63 μm) was analyzed using X-ray nephelometry with a Sedigraph 5100 grain size analyzer, except for core CGVIR-36 where the <250 μm fraction was analyzed to include all of the sample except some $CaCO_3$ shells, which were weighed separately. The Excel Macro GRADISTAT v.2.0 (Blott and Pye, 2001) was used to process the grain size data.

Total carbon (TC) and total inorganic carbon (TIC) were measured using a LECO CN-2000 and CC-100 carbon analyzer, respectively. $CaCO_3$ percentages were obtained from TIC values using a molecular weight ratio of 8.33. Total organic carbon (TOC) was calculated as TC–TIC. Total sulphur (TS) was measured in a Carlo-Erba CHNS-O EA

1108 elemental analyzer. The concentrations of 23 major and minor elements were determined by X-ray fluorescence (XRF) using a Siemens SRS 300 spectrometer in cores CGPL-00-6 and CGVIR-36. No samples from core ZV-1 were available for XRF measurements. Only Al, Ti, Fe (calculated as Al_2O_3, TiO_2 and Fe_2O_3), Mn and Ba data are presented here. The fraction of Ba controlled by diagenetic effects (Ba_{dia}) was estimated from standardized (mean=0, standard deviation=1) values of Ba, Al and TOC as $Ba_{dia}=Ba/(Al+TOC)$, where normalization to Al and TOC removes variability related to the fraction of Ba controlled by detrital material and biological productivity (e.g. Gingele et al., 1999).

Selected platinum-coated polished samples were observed using scanning electron microscopes (SEM) operating in back scattering mode (BS) using either a Philips XL 30 or a JEOL JSM-6700f SEM located in the Central Research Facilities unit of the University of Vigo. Magnetic mineral extracts were examined using JEOL JEM100CX transmission electron microscope (TEM) at the University of Munich. The energy dispersive X-ray spectroscopy (EDS) probe from each electron microscope was employed to semiquantitatively determine the chemical composition of relevant minerals. The 'bacteriodrome' at the University of Munich (Steinberger et al., 1994; Hanzlik et al., 2002), which consists of an optical microscope with three independently controlled sets of Helmholtz coils, was also employed to search for live magnetotactic bacteria in fresh surficial samples.

The mass-specific magnetic susceptibility (χ) was measured using a KLY-2 magnetic susceptibility bridge. The frequency dependence of χ (χ_{fd}) was measured as the percentage difference between measurements at 0.47 and 4.7 kHz using a Bartington Instruments MS2-B sensor. The isothermal and anhysteretic remanent magnetizations (IRM and ARM) were measured using an AGICO JR-5A spinner magnetometer and 2-G Enterprises cryogenic magnetometer. To generate the ARM, a dc bias field of 0.05 mT was superimposed on a decreasing alternating field (AF) with a peak value of 100 mT. The IRM was stepwise imparted in 15 steps up to a maximum field of 900 mT, which is referred to as $IRM_{900\,mT}$. The low $CaCO_3$ contents means that calculated carbonate-free magnetic parameters do not significantly depart from bulk measurements. Therefore, only bulk magnetic data will be discussed.

After measurements, the $IRM_{900\,mT}$ was demagnetized with a stepwise-applied back field up to -0.3 T to determine the coercivity of remanence (B_{cr}). The S-ratio at -0.3 T ($S_{-0.3\,T}$) was calculated according to the expression $S_{-0.3\,T}=[1-(IRM_{-300\,mT}/IRM_{900\,mT})]/2$

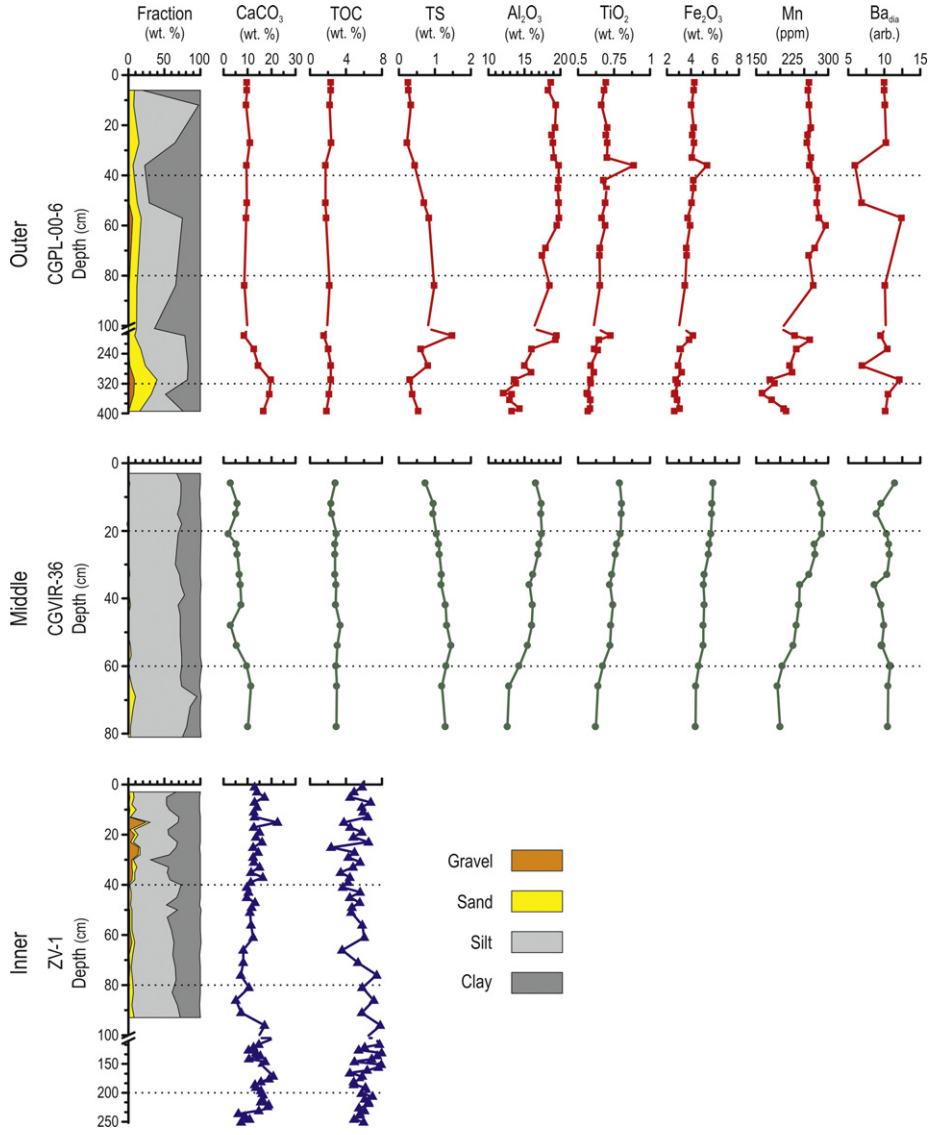

Fig. 2. Depth profiles of sediment textural and geochemical parameters for the studied cores. Note the axis breaks from 100 to 180 cm for core CGPL-00-6 and from 100 to 110 cm for core ZV-1, which are chosen to provide a detailed view of the uppermost part of these cores. The horizontal dotted lines are for comparison.

(Bloemendal et al., 1992). The hard IRM (HIRM) and medium IRM (MIRM) fractions of the $IRM_{900\,mT}$ were calculated as $HIRM = (IRM_{900\,mT} + IRM_{-300\,mT})/2$, $MIRM = (IRM_{900\,mT} + IRM_{-100\,mT})/2 - HIRM$, respectively (Yamazaki et al., 2003). The low IRM fraction (LIRM) was calculated as $LIRM = IRM_{900\,mT} - HIRM - MIRM$. The grain-size-sensitive ratio ARM/IRM was calculated at 100 mT for ARM and IRM so the same coercivity populations were magnetized. 72 selected samples were characterized in more detail by measuring hysteresis curves up to 1000 mT using a Princeton Measurements Corporation vibrating sample magnetometer (VSM) or alternating gradient magnetometer (AGM). Finally, thermomagnetic curves were measured up to 625 °C using a variable field translation balance (VFTB) in a magnetic field of 71 mT.

4. Results

4.1. Core descriptions

The texture of the studied cores is dominated by silty and clayey mud (Fig. 2). Sandy and gravely sediments typically account for less than 10% of the sediment, except in the lower part of core CGPL-00-6, where it reaches a maximum of ~40% at 320 cm. Occasional maxima in the gravel percentage in the studied cores, like those present above 30 cm in core ZV-1, are always associated with $CaCO_3$ bioclasts.

Sediment colour changes sharply from an uppermost brown interval (2.5Y 5/6), with thickness ranging from ~1 cm in cores ZV-1 and CGVIR-36 to 10 cm in core CGPL-00-6, to a dark grey/black zone (5Y 3/1–5Y 2-5/1) below this interval. X-radiographs (Fig. 3) do not contain indications of erosive marks or laminations. The only remarkable feature in the X-radiographs is the high density of elongated bright features (a few mm in length) that are embedded in the darker mud matrix (arrows in Fig. 3). These features occur below 215 cm in core CGPL-00-6 and below 82 cm in core ZV-1 but are absent in core CGVIR-36 and are interpreted to represent biogenic gas bubbles that acquired an elongated shape by coring-induced deformation. The presence of gas was confirmed by the characteristic H_2S smell noticed after core splitting.

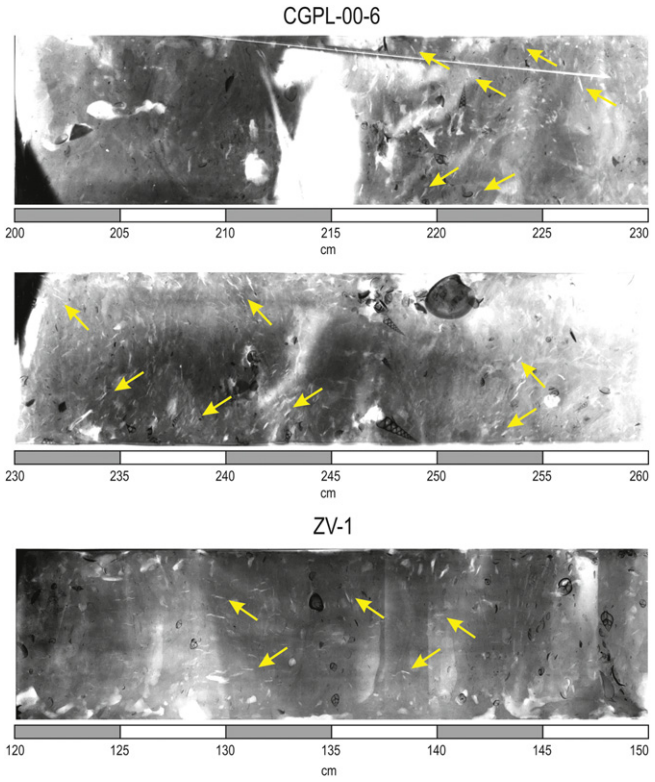

Fig. 3. X-ray radiographs of core sections from cores CGPL-00-6 and ZV-1 that span the intervals where gas bubbles (arrows) were detected within the sediments.

4.2. Sedimentation rates

According to the age model for core CGPL-00-6 (Table 1), sedimentation rates in the outer ria decreased from 100 cm/kyr at the base to 50 cm/kyr at the top of the core. In the inner ria, sedimentation rates are 2–4 times higher, and reach values of 180 cm/kyr in core ZV-1 (Muñoz Sobrino et al., 2007).

4.3. Geochemistry

$CaCO_3$ in the studied cores is exclusively biogenic, and occurs in the form of shell fragments. Average $CaCO_3$ contents (Fig. 2) are low, ranging between 6% and 14% with slight down-core increases in all of the cores.

TOC (Fig. 2) decreases down-core in core CGPL-00-6 from 2.3% to 1.6% with a distinct drop at 35 cm. An increase to surficial TOC values is observed below 190 cm, close to the interval where gas bubbles are observed. In the middle and inner ria, TOC increases down-core, from 2.8% to 3.4% in core CGVIR-36 and from 5% to 8% in core ZV-1. TS increases down-core from 0.5% to 0.6% near the surface to maxima of ~2% (Fig. 2). The maximum TS content is observed in core CGPL-00-6 at 190 cm, close to the first occurrence of gas bubble marks in the X-radiographs. Unfortunately, no TS data are available for core ZV-1 to confirm the association of gas with high TS contents in this core. Both TOC and TS increase toward the inner part of the ria, which is in agreement with published results for surficial sediments (Vilas et al., 1995).

The terrigenous components Al_2O_3 and TiO_2 (Fig. 2) decrease gradually with depth; only two moderate TiO_2 peaks occur at 35 and 200 cm in core CGPL-00-6. The redox-sensitive Fe_2O_3 and Mn (Fig. 2) undergo an overall decrease down-core, with Mn being relatively constant until ~20 cm in core CGVIR-36 and until ~60 cm in core CGPL-00-6. This may indicate an increase in anoxic conditions below this depth. The exception to the down-core decreasing trend is a small peak at 190 cm in core CGPL-00-6. This peak possibly marks

Table 1
^{14}C AMS dates for core CGPL-00-6.

Depth (cm)	^{14}C AMS date	Calendar years	Calibrated BP	Local reservoir effect
45	854 ± 75	1293–1678 AD	272–657	-7 ± 90 (Soares, 1993)
230	2752 ± 59	719–381 BC	2330–2668	–

Calibrated ages are 2σ ranges.

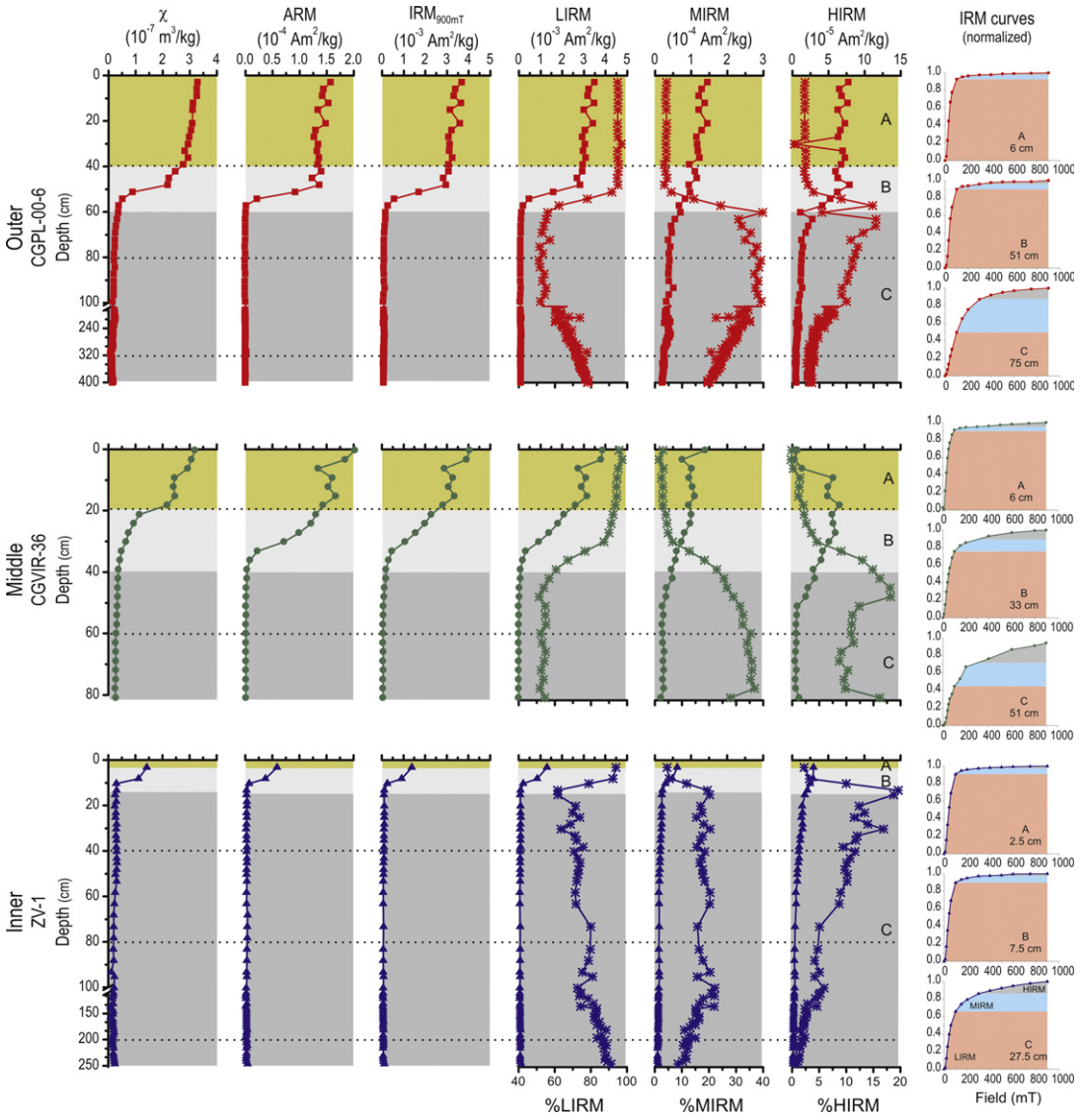

Fig. 4. Down-core profiles of concentration-dependent magnetic properties for the three studied cores. The asterisks in the LIRM (low), MIRM (medium) or HIRM (hard IRM) plots represent the percentage of remanence carried by the respective fraction. Note the axis breaks from 100 to 180 cm for core CGPL-00-6 and from 100 to 110 cm for core ZV-1, which are chosen to provide a detailed view of the uppermost part of these cores. The coloured intervals represent zones A, B and C for each core. The horizontal dotted lines are for comparison. Representative IRM curves for each zone are shown to the right of the corresponding down-core profiles. Orange shading highlights the IRM fraction acquired below 100 mT (LIRM), blue shading corresponds to the IRM fraction acquired from 100 to 300 mT (MIRM) and grey shading represents the IRM acquired at fields higher than 300 mT (HIRM).

the position of an ancient redox front, where dissolved reduced Mn produced in underlying anoxic sediments migrated upward and precipitated under formerly suboxic conditions at this depth. Ba_{dia} has minima at 40 and 250 cm in core CGPL-00-6 and at 12 and 39 cm in core CGVIR-36 (Fig. 2).

4.4. Magnetic properties

4.4.1. Concentration-dependent magnetic properties

All of the cores studied have similar down-core decreasing χ, ARM and $IRM_{900\ mT}$ profiles (Fig. 4) with high values in the upper part of the cores and low and stable values below depths of 60, 40 and 10 cm for cores CGPL-00-6, CGVIR-36 and ZV-1, respectively. These magnetic properties correlate with the detrital proxies Al_2O_3 and TiO_2 (Table 2). However, the similarity of TiO_2-normalized magnetic data (Fig. 5) suggests that detrital variations are not the main driver of the observed χ, ARM and $IRM_{900\ mT}$ behaviour with depth.

Based on the similar concentration-dependent magnetic properties, we define a three layer magnetic zonation (Fig. 4). The depth range of each zone and the average and range of χ, ARM and $IRM_{900\ mT}$ values are summarized in Table 3.

Zone A is the uppermost interval, and is characterized by the highest χ, ARM and $IRM_{900\ mT}$ values that gradually decrease with depth with the exception of the local minimum at 15 cm in core CGVIR-36. The intermediate zone B is marked by steep gradients in χ, ARM and $IRM_{900\ mT}$, with a 45–80% reduction compared to the respective maxima in zone A. The lowermost zone C is characterized by low and stable values of χ, ARM and $IRM_{900\ mT}$. χ decreases between 85% and 93% in zone B compared to zone A, while for ARM and IRM the decline is 95–99%. ARM is the most affected by this decrease, with values that are 99% lower in cores CGPL-00-6 and CGVIR-36, and 95% lower in core ZV-1. From a spatial perspective, χ, ARM and $IRM_{900\ mT}$ increase from the inner ria to the middle/outer ria. Zones A and B are also thicker in the outer ria with maximum thicknesses reaching 40 and 20 cm, respectively, in core CGPL-00-6.

Table 2
Pearson correlation coefficients between concentration-dependent magnetic properties and textural and compositional parameters.

	χ	ARM	$IRM_{900\ mT}$	LIRM	MIRM	HIRM
CGPL-00-6						
Sand	**−0.55***	**−0.54***	**−0.55***	**−0.54***	**−0.62***	**−0.61***
Silt	−0.13	−0.19	−0.16	−0.16	−0.15	−0.18
Clay	0.33	0.39	0.35	0.35	0.37	0.38
$CaCO_3$	−0.42	−0.42	−0.42	−0.42	**−0.55***	**−0.55***
TOC	0.24	0.17	0.20	0.20	0.11	0.02
Al_2O_3	**0.55***	**0.57***	**0.57***	**0.56***	**0.7***	**0.73***
TiO_2	**0.62***	**0.62***	**0.62***	**0.62***	**0.66***	**0.68***
Fe_2O_3	**0.75***	**0.76***	**0.76***	**0.75***	**0.81***	**0.82***
Mn	0.50	0.53	0.52	0.51	**0.67***	**0.7***
TS	**−0.56***	**−0.55***	**−0.56***	**−0.57***	−0.46	−0.44
Ba_{dia}	−0.27	−0.21	−0.23	−0.24	−0.21	−0.12
CGVIR-36						
Sand	−0.11	−0.15	−0.15	−0.15	−0.20	−0.35
Silt	−0.25	−0.34	−0.33	−0.33	−0.43	−0.50
Clay	0.30	0.43	0.42	0.41	0.54	**0.69***
$CaCO_3$	−0.51	−0.57	−0.56	−0.55	**−0.62***	−0.50
TOC	**−0.69***	**−0.7***	**−0.72***	**−0.72***	**−0.68***	−0.54
Al_2O_3	**0.63***	**0.71***	**0.7***	**0.7***	**0.8***	**0.8***
TiO_2	**0.76***	**0.81***	**0.81***	**0.81***	**0.88***	**0.75***
Fe_2O_3	**0.85***	**0.88***	**0.88***	**0.88***	**0.92***	**0.69***
Mn	**0.76***	**0.86***	**0.85***	**0.84***	**0.94***	**0.85***
TS	**−0.92***	**−0.86***	**−0.89***	**−0.89***	**−0.88***	−0.45
Ba_{dia}	**0.78***	**0.77***	**0.79***	**0.79***	**0.71***	0.46
ZV-1						
Sand	0.09	0.21	0.25	0.25	0.30	0.26
Silt	−0.02	0.05	0.01	0.02	−0.10	−0.27
Clay	0.08	0.00	0.02	0.02	0.07	0.15
$CaCO_3$	−0.03	0.00	0.02	0.01	0.11	0.36
TOC	0.08	0.05	0.06	0.05	0.10	0.22

* Indicates correlations that are significant at the 95% confidence level ($p < 0.05$).

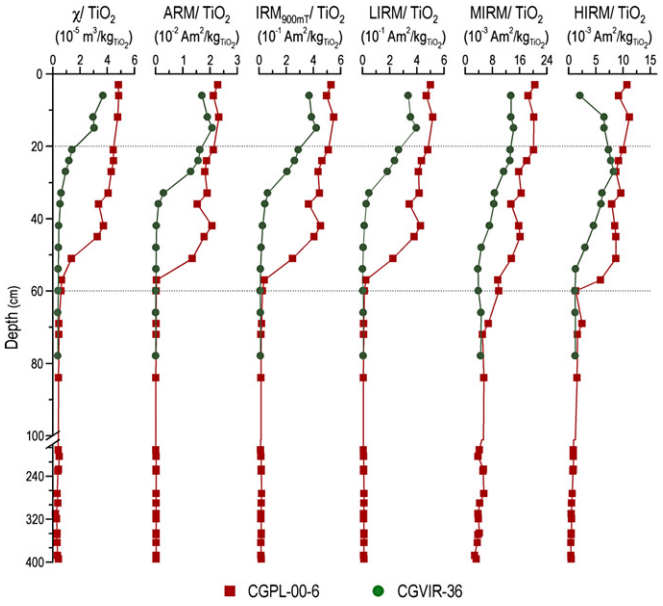

Fig. 5. Down-core variation of the TiO_2-normalized concentration-dependent magnetic parameters. Note the depth axis break from 100 cm to 180 cm.

4.4.2. Magnetic mineralogy

Representative thermomagnetic curves for eight samples from zones A and B of cores CGPL-00-6 and CGVIR-36 are shown in Fig. 6. Low magnetic intensity samples from the lower parts of zone B and zone C have noisy signals. All of the samples undergo a marked magnetization increase above 400–450 °C, with a peak at ~500 °C and a subsequent drop to near-zero values at ~580 °C. Considering the high TS contents and SEM observation of Fe sulphides (discussed in Section 4.5) in the studied cores, this behaviour is best explained by the oxidation of pyrite to magnetite (Roberts and Pillans, 1993; Passier et al., 2001). The production of magnetite during heating precludes identification of other sources of magnetite in the thermomagnetic curves.

Samples from zone A from cores CGPL-00-6 and especially CGVIR-36 undergo a small drop in magnetization at ~250 °C, and a subsequent minor increase that peaks at ~300 °C (Fig. 6). This feature may be caused by greigite, which has been shown to thermally break down above 270 °C. The subsequent peak may be caused by the reported production of minor amounts of pyrrhotite above 282 °C (Skinner et al., 1964). Further heating produces magnetite, which contributes to the observed peak at ~450 °C (Krs et al., 1992; Roberts, 1995; Geiss and Banerjee, 1997; Dekkers et al., 2000; Liu et al., 2004; Chang et al., 2008).

The coercivity-related parameters B_{cr} and $S_{-0.3\,T}$ mirror the down-core patterns of the concentration-dependent magnetic properties (Fig. 7; Table 4). Magnetite is the main magnetic mineral in zone A, as indicated by B_{cr} values of 15–35 mT, S-ratios higher than 0.95 and IRM acquisition curves approaching saturation at fields < 100 mT (Fig. 4). B_{cr} increases sharply in the lower part of zone B, and reaches maximum values of 61–80 mT that remain relatively stable with depth. This coercivity increase, along with IRM acquisition curves that do not saturate at 900 mT (Fig. 4), confirm the presence of hematite in zones B and C. Hematite contents may represent as much as 80% of the magnetic mineral content as indicated by $S_{-0.3\,T}$ values lower than 0.88 (Bloemendal et al., 1993). Greigite also has a higher B_{cr} value than magnetite (Roberts, 1995), and therefore will also contribute to this coercivity increase. Therefore, the estimated contribution of hematite based on the $S_{-0.3\,T}$ must be regarded as an upper limit assuming negligible greigite contribution. A down-core decreasing B_{cr} trend is observed in zone C for the longer cores ZV-1 and especially CGPL-00-6.

LIRM, MIRM and HIRM (Fig. 4 and Table 3) also depend on the relative concentration of magnetic minerals with different coercivities, and therefore have similar profiles as χ, ARM and $IRM_{900\ mT}$. LIRM represents 93–95% of $IRM_{900\ mT}$ in zone A, as illustrated by IRM curves (Fig. 4). This high LIRM contribution highlights the predominance of low coercivity minerals in zone A. Below zone A, the proportion of low coercivity minerals decreases significantly, with LIRM dropping to 55–78% and MIRM increasing from 2% to 4% in zone A to 14–30% in zone C. HIRM also increases, with its maximum contribution in zone C reaching 14% in core CGVIR-36. The non-detrital MIRM ($MIRM/TiO_2$) subtly increases at 190 cm, close to the first occurrence of gas bubbles in core CGPL-00-6 (Fig. 5), which suggests a possible role for anaerobic oxidation of methane (AOM) in this coercivity increase. Cores CGPL-00-6 and ZV-1 are further characterized by a progressive down-core increase in the LIRM contribution within zone C, which is reflected in the associated B_{cr} decrease below 190 cm, especially in core CGPL-00-6. This difference with core CGVIR-36 may be explained by the longer length of these cores, which enables resolution of this feature.

4.4.3. Magnetic grain size

Zone A is characterized by relatively stable χ_{fd} of around 7–8% (Fig. 7; Table 4) for cores CGPL-00-6 and CGVIR-36 and 3.5% for ZV-1, which indicates a moderate-high contribution of super-paramagnetic (SP) particles (< 0.03 μm for magnetite). This SP contribution can be caused by nucleation of SP greigite as early

Table 3
Mean values ±1 standard deviation and ranges of concentration-dependent magnetic properties for the three zones defined for each studied core.

Core	Zone	χ (10^{-7} m^3/kg)	ARM (10^{-4} A m^2/kg)	$IRM_{900\ mT}$ (10^{-3} A m^2/kg)	LIRM (10^{-3} A m^2/kg)	MIRM (10^{-4} A m^2/kg)	HIRM (10^{-5} A m^2/kg)
CGPL-00-6	**A (0–40 cm)**	3.1 ± 1.7 (2.8–3.3)	1.4 ± 0.1 (1.3–1.6)	3.3 ± 0.2 (3.1–3.7)	3.1 ± 0.2 (2.9–3.5)	1.2 ± 0.1 (0.9–1.4)	6.1 ± 1.9 (0.1–7.5)
	B (40–60 cm)	1.3 ± 1.0 (0.4–2.5)	0.7 ± 0.6 (0.1–1.4)	1.6 ± 1.3 (0.2–3.1)	1.5 ± 1.3 (0.1–2.9)	0.9 ± 0.2 (0.6–1.1)	5.0 ± 2.1 (0.9–7.7)
	C (> 60 cm)	0.2 ± 0.1 (0.1–0.4)	0.0 ± 0.1 (0.0–0.1)	0.1 ± 0.1 (0.0–0.2)	0.0 ± 0.1 (0.0–0.1)	0.3 ± 0.1 (0.2–0.5)	0.6 ± 0.3 (0.2–2.6)
CGVIR-36	**A (0–20 cm)**	2.7 ± 0.4 (2.1–3.2)	1.6 ± 0.2 (1.4–2.0)	3.4 ± 0.5 (2.8–4.1)	3.2 ± 0.5 (2.7–3.9)	1.1 ± 0.2 (0.8–1.4)	3.8 ± 2.6 (0.6–6.9)
	B (20–40 cm)	0.7 ± 0.3 (0.3–1.1)	0.7 ± 0.5 (0.1–1.3)	1.1 ± 0.9 (0.2–2.3)	1.0 ± 0.8 (0.1–2.1)	0.8 ± 0.2 (0.5–1.1)	5.1 ± 1.1 (3.2–6.3)
	C (> 40 cm)	0.3 ± 0.1 (0.2–0.3)	0.0 ± 0.1 (0.0–0.1)	0.1 ± 0.01 (0.0–0.2)	0.0 ± 0.1 (0.0–0.1)	0.3 ± 0.1 (0.2–0.5)	1.3 ± 0.8 (0.7–3.4)
ZV-1	**A (0–3 cm)**[a]	1.4	0.6	1.4	1.3	0.6	2.8
	B (4–15 cm)	0.5 ± 0.4 (0.3–1.1)	0.1 ± 0.2 (0.0–0.4)	0.3 ± 0.4 (0.1–0.9)	0.3 ± 0.4 (0.1–0.8)	0.3 ± 0.1 (0.2–0.5)	2.2 ± 0.5 (1.7–2.8)
	C (> 15 cm)	0.2 ± 0.1 (0.1–0.3)	0.0 ± 0.1 (0.0–0.1)	0.0 ± 0.1 (0.0–0.1)	0.0 ± 0.1 (0.0–0.1)	0.1 ± 0.1 (0.0–0.2)	0.4 ± 0.4 (0.1–1.4)

[a] Zone A in core ZV-1 only comprises one sample.

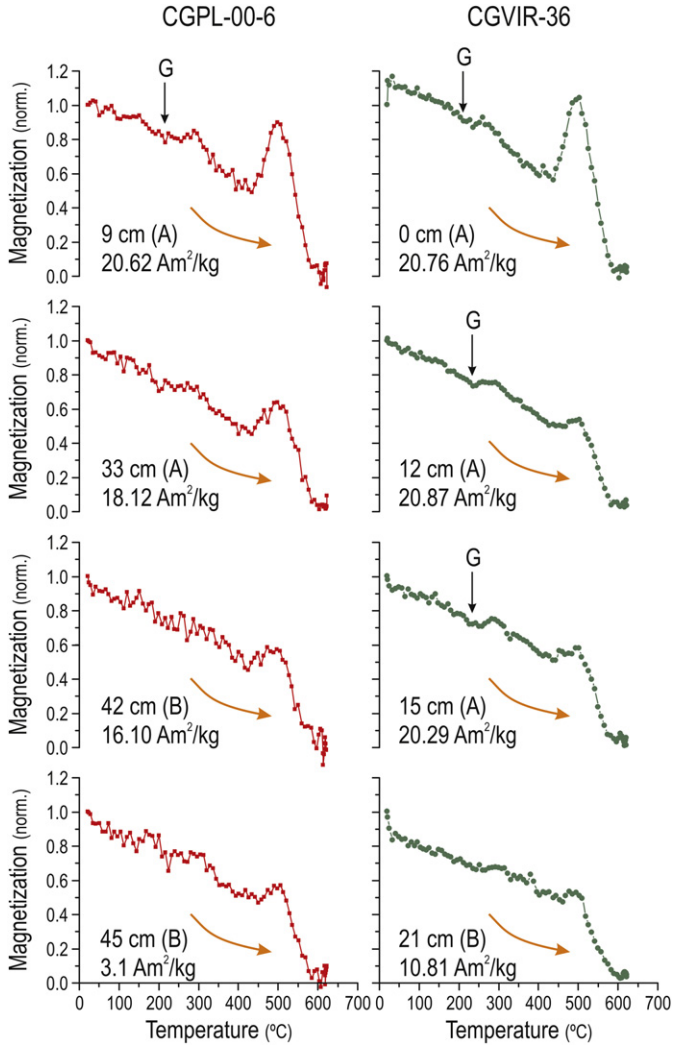

Fig. 6. Magnetization as a function of increasing temperature up to 625 °C for selected samples from zones A and B in cores CGPL-00-6 and CGVIR-36. The curved arrows indicate heating. Data were normalized to the initial magnetization value. Initial magnetizations are indicated for each curve below its corresponding depth. Letters in parenthesis indicate the diagenetic zone from which the sample is located. The vertical arrows indicate features that are interpreted as greigite (G) thermal alteration.

diagenesis progresses (Tarduno, 1995; Rowan et al., 2009). A marked decrease in χ_{fd} is observed in zone B of core CGPL-00-6, which suggests a rapid removal of fine-grained material. Below this interval and in zones B and C of the rest of the cores, χ_{fd} measurements are unreliable due to low signal-to-noise ratio that results from the weak magnetic susceptibility values.

The ARM/IRM ratio is controlled by ferrimagnetic minerals and is usually interpreted as a grain size indicator for magnetic mineral assemblages dominated by magnetite (Thompson and Oldfield, 1986; Maher, 1988; Evans and Heller, 2003). Two main features are evident in the down-core evolution of this parameter. Zone B is characterized by a marked increase, which is interpreted as a fining of grain size in the magnetic mineral assemblages. This increase can also be caused by greigite, which often exhibits SD behaviour (Roberts, 1995). $IRM_{900\ mT}/\chi$ maxima of 25–30 kA/m at the same depths also suggest the presence of greigite (e.g. Snowball, 1991; Roberts and Turner, 1993; Roberts, 1995; Sagnotti and Winkler, 1999). This increase reverses within zone B, and reaches its lowest values in all of the cores at the top of zone C. This ARM/IRM decrease is indicative of a coarsening of the mean magnetic grain size, which is maintained throughout zone C.

In a Day diagram (Day et al., 1977) the samples plot mostly within the PSD (pseudo-single domain) region (Fig. 8), which corresponds to a grain size range of 1–15 μm for magnetite. Data for samples located deeper in the cores have a trend toward the MD (multi-domain) end-member. The data also fall within the region defined by mixing-models for single domain (SD)+MD and SD+SP grains (Dunlop, 2002) and have a trend similar to SD+SP mixing lines. This is consistent with the observation of SD bacterial magnetosomes and MD-sized detrital Fe oxides (see Section 4.5 below). The offset toward higher B_{cr}/B_c values may be caused by contrasting coercivities associated with the relative increase in coercivity below zone A (Wasilewski, 1973; Day et al., 1977; Nagata and Carleton, 1987). Alternatively, the offset from the SD+MD mixing line suggests an increased contribution from SP particles, similar to the results obtained by Rowan et al. (2009) in cores from the Oman and Californian margins. These authors identified a counter-clockwise trend that is common in reductive diagenetic environments, and which is characterized by an initial shift toward MD values that is caused by the almost complete dissolution of detrital SD and PSD (titano-)magnetite, followed by a trend toward SD behaviour caused by nucleation of SP greigite and continued growth to SD size as diagenesis progresses. Our results indicate the opposite behaviour, with an initial trend toward SD values, which we interpret as due to an increased contribution from SD greigite. Deeper in the cores, the data plot toward the MD region of the Day plot, which we interpret as resulting from a lower contribution from greigite due to intense anoxic conditions and progressive pyritization. The lack of a counter-clockwise loop back to SD-like values with depth (cf. Rowan et al., 2009) reflects the lack of significant greigite growth from SP to SD size in zone C of these cores.

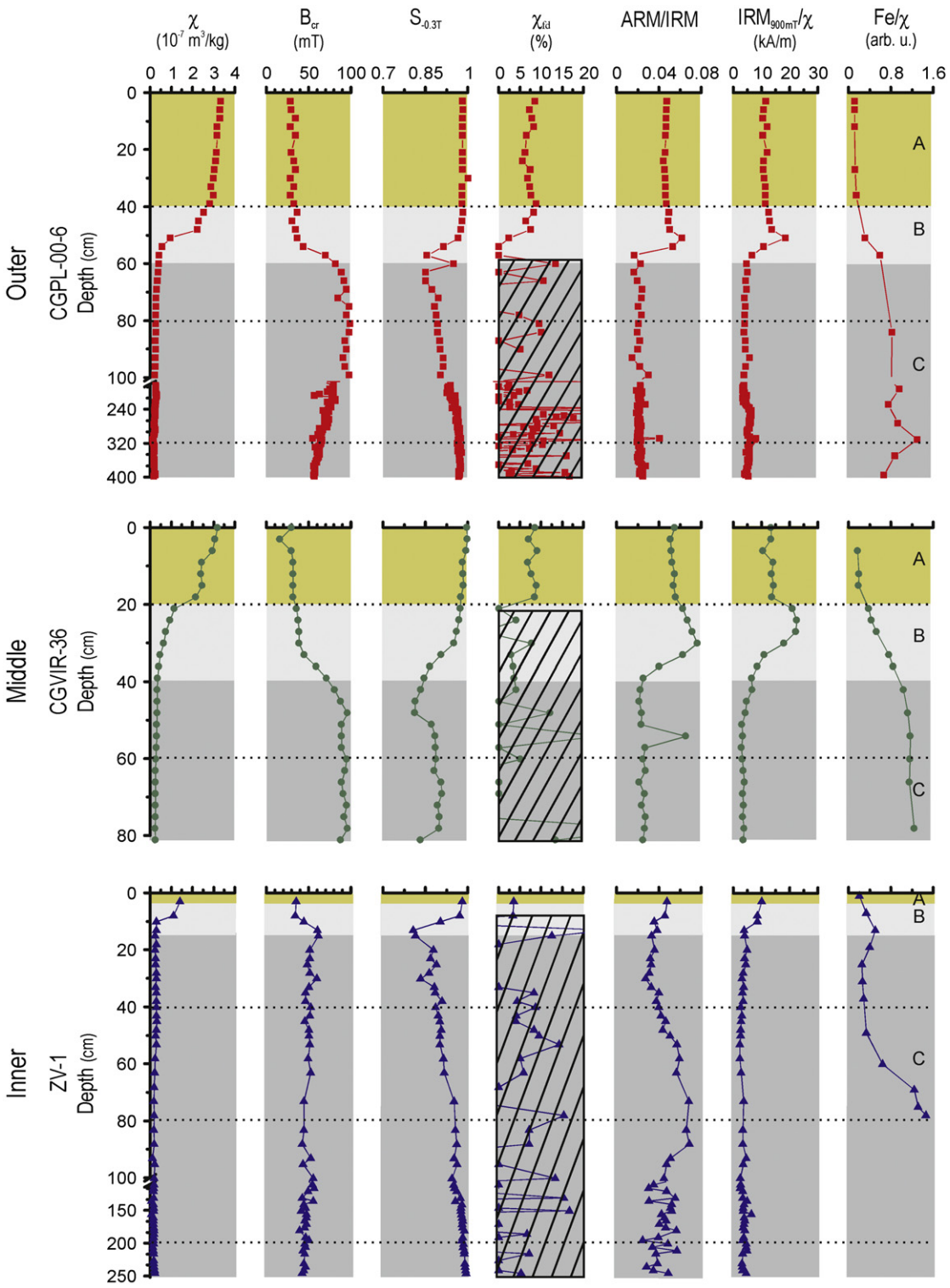

Fig. 7. Down-core plots of the concentration-independent magnetic parameters. χ is presented for comparison. Note the axis breaks from 100 to 180 cm for core CGPL-00-6 and from 100 to 110 cm for core ZV-1, which are chosen to provide a detailed view of the uppermost part of the cores. The coloured intervals represent zones A, B and C for each core. The hatched areas in the χ_{fd} plots highlight zones where χ_{fd} is not reliable due to low magnetic susceptibilities. The horizontal dotted lines are for comparison.

4.5. Electron microscopy

The described magnetic property zonation is also evident in SEM observations. Zone A sediments have a high abundance of large detrital Fe oxides (Fig. 9a, b). TEM images of magnetic extracts reveal the occurrence of bacterial magnetosomes in the upper interval of this zone (Fig. 9c). Most detrital magnetic minerals bear clear signs of dissolution (arrows in Fig. 9a, b), which, along with significant amounts of framboidal Fe sulphides (Fig. 9d), indicates the onset of reducing conditions in zone A.

Table 4
Mean values ±1 standard deviation and ranges of concentration-independent magnetic properties for the three zones defined for each studied core.

Core	Zone	χ_{fd} (%)	B_{cr} (mT)	$S_{-0.3\,T}$	ARM/IRM	$IRM_{900\,mT}/\chi$ (kA/m)
CGPL-00-6	**A (0–40 cm)**	7.3 ± 1.0 (5.6–8.8)	30.7 ± 2.6 (28.0–34.0)	0.98 ± 0.01 (0.98–1.00)	0.05 ± 0.00 (0.04–0.05)	10.7 ± 0.5 (10.0–11.5)
	B (40–60 cm)	5.4 ± 4.9 (0.0–13.3)	47.0 ± 19.8 (30.0–81.0)	0.95 ± 0.05 (0.86–0.98)	0.04 ± 0.02 (0.02–0.06)	10.9 ± 4.6 (4.2–18.1)
	C (>60 cm)	6.8 ± 11.2 (−16.7–35.0)	73.9 ± 13.1 (54.0–98.0)	0.94 ± 0.03 (0.85–0.98)	0.02 ± 0.00 (0.01–0.04)	4.5 ± 0.9 (2.9–7.5)
CGVIR-36	**A (0–20 cm)**	8.0 ± 0.9 (6.8–9.0)	28.1 ± 5.9 (15.0–31.0)	0.99 ± 0.01 (0.98–1.00)	0.05 ± 0.00 (0.05–0.05)	12.8 ± 1.3 (10.0–13.8)
	B (20–40 cm)	2.5 ± 3.6 (−3.9–7.7)	45.7 ± 13.3 (35.0–70.0)	0.92 ± 0.05 (0.85–0.97)	0.06 ± 0.02 (0.02–0.08)	15.1 ± 6.8 (6.1–21.9)
	C (>40 cm)	4.6 ± 13.1 (−17.6–35.3)	89.8 ± 4.1 (80.0–95.0)	0.87 ± 0.03 (0.81–0.91)	0.03 ± 0.01 (0.02–0.06)	3.3 ± 1.0 (2.5–6.2)
ZV-1	**A (0–3 cm)**[a]	3.5	35.0	0.98	0.05	9.7
	B (4–15 cm)	4.7 ± 20.9 (−23.3–26.3)	49.7 ± 13.1 (34.0–61.0)	0.87 ± 0.08 (0.81–0.97)	0.04 ± 0.01 (0.03–0.05)	5.9 ± 2.7 (3.4–8.3)
	C (>15 cm)	−1.4 ± 12.2 (−46.1–16.7)	47.7 ± 4.3 (39.0–59.0)	0.94 ± 0.04 (0.83–0.99)	0.04 ± 0.01 (0.02–0.07)	3.2 ± 0.8 (1.9–6.1)

[a] Zone A in core ZV-1 only comprises one sample.

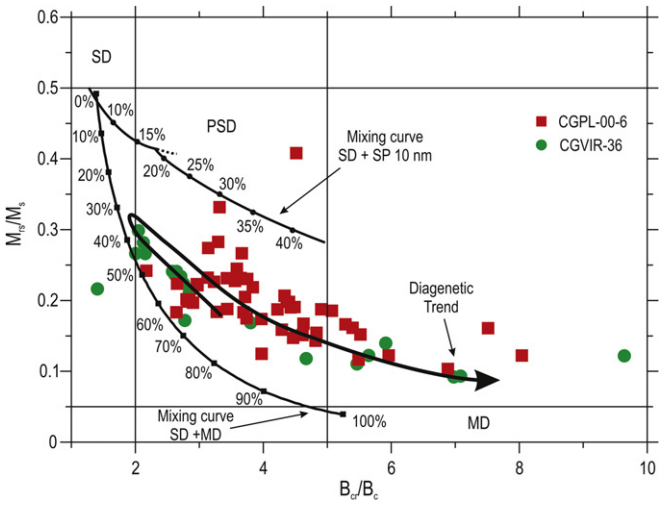

Fig. 8. Hysteresis parameters for the studied cores represented in a Day plot (Day et al., 1977) along with the SD+SP and SD+MD mixing lines proposed by Dunlop (2002). The arrow indicates the overall trend of the data with depth in the cores.

However, the Fe sulphides occur mainly in organic-rich microenvironments (faecal pellets, bioclasts, etc.) where highly reducing conditions occur locally. These sulphides have Fe/S atomic ratios that range from 0.5, corresponding to pyrite, to 0.75, which is typical of greigite. Greigite-like ratios are more common in the smaller particles with lower electron backscatter (Fig. 9e). Greigite aggregates usually appear darker compared to pyrite as a result of dispersion of the electron beam after interacting with the smaller crystallites in greigite aggregates (Roberts and Weaver, 2005). Deeper in zone B and in all of zone C, Fe sulphides are ubiquitous and often appear within the layers of phyllosilicates (Fig. 9f). This feature is usually an indication of long-lasting anoxic-sulphidic conditions (Canfield et al., 1992; Jiang et al., 2001; Roberts and Weaver, 2005). However, our results suggest that in organic-rich shallow coastal sediments this process can occur in time-scales of less than 10 kyr.

5. Discussion

5.1. Early diagenesis

The significant negative correlation between TOC and TS, which reflects the concentration of diagenetically produced Fe sulphides, and concentration-dependent magnetic parameters (Table 2), especially in core CGVIR-36, suggests that reductive early diagenesis caused by the microbial oxidation of organic matter in the sediments is responsible for the observed magnetic mineral depletion with depth. Lack of a significant correlation between TOC and the magnetic properties in core ZV-1 may be explained by rapid dissolution of magnetic minerals in the uppermost part of the core that results from the large TOC concentration in this core.

The Fe_2O_3 and Mn records only contain subtle features (e.g. an Fe_2O_3 peak at 40 cm in CGPL-00-6 and a Mn peak at 20 cm in CGVIR-36; Fig. 2), which can be interpreted as former redox boundaries. Changes in sediment colour from brown to greenish-grey are interpreted as the transition from oxic to suboxic/anoxic sedimentary conditions (Lyle, 1983), where Fe^{3+} is reduced before sulphate reduction and methanogenesis starts (Froelich et al., 1979). These changes occur within 1 cm of the sediment surface in inner and middle ria settings, and at ~10 cm depth in the outermost ria. The shallow depth of this transition, which occurs well within zone A in all cores, indicates strongly reducing conditions in all cores and a shallow position for the active Mn and Fe redox boundaries which would explain the lack of a clear redox signature for these elements. The difference in the depth of the colour change among the cores highlights the contrasting intensities of early diagenesis in sediments from the Ria de Vigo.

The occurrence of framboidal and other sulphide aggregates throughout the studied cores indicates that sulphate reduction occurs at all depths. However, in zone A the confinement of these sulphides to within organic-rich microenvironments suggests that anoxic conditions are not pervasive within this zone. Under severely anoxic conditions in the underlying sediments, sulphate reduction also causes dissolution of the otherwise insoluble $BaSO_4$ (Kasten and Jørgensen, 2000). We have used the Ba_{dia} index to detect the establishment of anoxic sulphidic conditions. A minimum in Ba_{dia} occurs at the bottom of zone A (Fig. 2). This suggests that Ba_{dia} responds earlier to sulphate reduction than the magnetic properties, probably because magnetic minerals are affected by the build-up of H_2S as a result of sulphate reduction, whereas barite would be directly dissolved during sulphate reduction. Based on the location of this Ba_{dia} minimum, zone B and the lower part of zone A can be considered to be anoxic sulphidic, according to the classification of Berner (1981). In the methanogenic zone of core CGPL-00-6 below 190 cm, Ba_{dia} has a similar minimum. This minimum is probably caused by barite dissolution associated with sulphate reduction at the sulphate–methane transition zone (Froelich et al., 1979).

5.2. Diagenetic zonation of magnetic minerals

The above interpretations and SEM evidence for significant dissolution of detrital magnetic grains and iron sulphide formation (Fig. 9) indicate that the main process that controls the

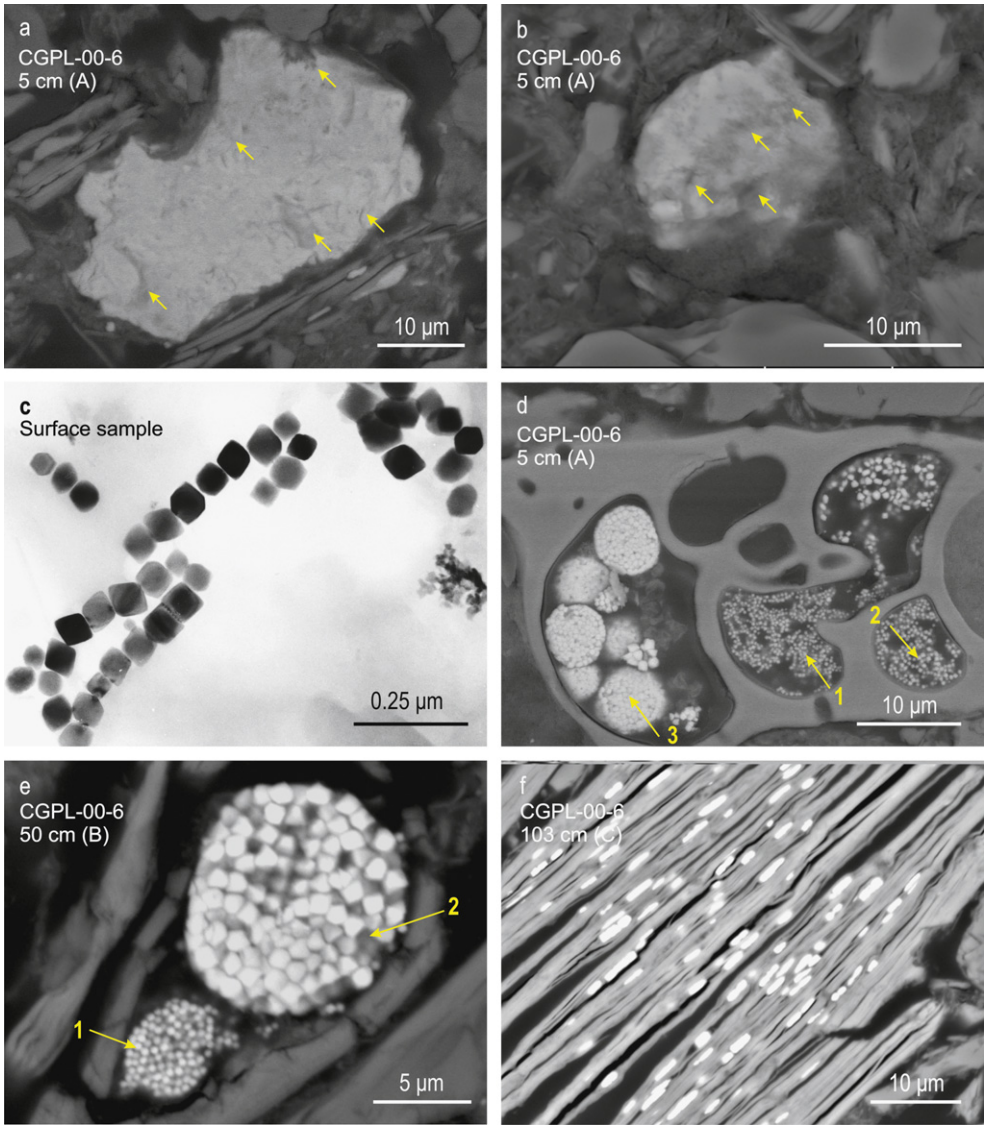

Fig. 9. SEM back-scatter micrographs of representative samples from the different diagenetic zones identified in this study in core CGPL-00-6: (a) large Fe oxide with dissolution pits on its surface. The Fe:Ti:O content determined by EDS was 28:0:72, (b) large Fe oxide with dissolution pits and a Fe:Ti:O composition of 42:0:58, which is similar to the ratio for magnetite (43:0:57), (c) TEM image of chains of bacterial magnetosomes in a sample of surface sediments from the Ria de Vigo, (d) framboidal sulphides within an organic-rich carbonate microenvironment. The sulphide composition ranges from pure pyrite to greigite. The Fe/S ratios of the analyzed aggregates were 1: 0.72; 2: 0.72; 3: 0.64, (e) detail of a framboidal Fe sulphide (1) with Fe/S ratio of 0.74, which is indicative of greigite. The Fe/S ratio of the adjacent minerals (2) was 0.57, which is closer to that of pyrite, (f) authigenesis of Fe sulphides within the exfoliation planes of phyllosilicates. All but the TEM image are from core CGPL-00-6. The respective diagenetic zone (A, B or C) is shown in parenthesis after the sample depth.

observed vertical magnetic zonation in the studied cores is reductive dissolution of magnetic iron oxides. Zone A is characterized by mild reducing conditions that have not generally progressed to the anoxic/sulphidic stage. The occurrence of Fe sulphides in this zone is restricted to the environs around decomposing organic remains, where intense reducing conditions are localized, and therefore do not significantly affect the overall magnetic properties of this zone. Bacterial reduction of Fe oxides in the surrounding sediments would have produced Fe^{2+}, which could then diffuse inside these microenvironments and precipitate as Fe sulphides. Zone A does not contain any ARM/IRM and/or $IRM_{900\ mT}/\chi$ related evidence of magnetic coarsening, which is generally associated with preferential dissolution of smaller minerals during reductive diagenesis (Karlin and Levi, 1983).

In zone B, development of anoxic/sulphidic conditions is indicated by the ubiquitous precipitation of Fe sulphides, increased TS, and Ba_{dia} peaks just above this zone (Fig. 2). In such highly reducing environments, magnetic oxides and oxyhydroxides are rapidly dissolved (Canfield et al., 1992; Haese, 2000). This dissolution, and especially removal of magnetite, explains the large decrease in concentration-dependent magnetic parameters that are characteristic of this zone. The decrease in χ also explains the increased Fe/χ in this zone (Fig. 7), which is driven by the fact that the χ loss is not balanced by a proportional decrease in Fe, which remains in zone B due to ubiquitous framboidal pyrite precipitation.

The large LIRM decrease compared to HIRM in zone B (Fig. 4) indicates a relative increase in the proportion of high-coercivity goethite and/or hematite, which are widely documented as more resistant to anoxic/sulphidic conditions in both coastal (Liu et al., 2004; Emiroğlu et al., 2004; Rey et al., 2005; Kawamura et al., 2007) and offshore environments (Bloemendal et al., 1993; Robinson et al., 2000; Yamazaki et al., 2003; Garming et al., 2005; Rowan et al., 2009), despite their higher reported reactivity

toward HS^- (Canfield et al., 1992; Haese, 2000). This apparent contradiction is often explained assuming hematite is larger than magnetite. However, observation of this coercivity increase in many different environments, particularly in deep-sea environments with efficient grain sorting and narrow grain size distributions makes this assumption unrealistic. Differences in sorption chemistry kinetics between HS^- and other seawater solutes have been proposed to explain the lower reactivity of hematite compared to magnetite (Poulton et al., 2004). Dissolution of these minerals by HS^- occurs by surface complexation during which other seawater solutes may block available complexation sites and reduce the dissolution rate. Differences in surface area between these minerals, coupled with differential competition and mineral reactivities, result in increased reactivity of magnetite compared to hematite (Poulton et al., 2004). This relative increase in hematite and/or goethite with depth also explains the high B_{cr}, %HIRM and S-ratios that are characteristic of zone B.

The magnetic grain size fining suggested by ARM/IRM and $IRM_{900\,mT}/\chi$ in the upper half of zone B (Fig. 7) is an uncommon feature that deserves attention because reductive dissolution of magnetic oxides will typically cause a magnetic coarsening due to preferential removal of finer particles due to their higher surface area to volume ratio (e.g. Karlin and Levi, 1983; Leslie et al., 1990; Bloemendal et al., 1992; Yamazaki et al., 2003; Rey et al., 2005). The ARM/IRM fining occurs well within the anoxic zone of the sediments, which makes it unlikely to be caused by production of bacterial magnetite at this level. Authigenic greigite often has SD characteristics (Snowball, 1991; Roberts, 1995) and SEM results confirm the occurrence of greigite in this zone. Therefore, we interpret this fining to result from a relative increase in the proportion of greigite associated with rapid dissolution of (titano-)magnetite. Greigite magnetosomes are usually found in sulphate-reducing sediments (Mann et al., 1990; Stolz, 1993; Posfai et al., 2001; Simmons et al., 2004; Vasiliev et al., 2008), and may also contribute to the observed ARM/IRM increase in this zone. No magnetic extracts were available for TEM observations from this zone to verify their existence. Below this peak, we interpret the observed magnetic coarsening to result from transformation of greigite into pyrite, which would be favoured by the intense anoxic conditions and high TOC. The loss of SD greigite would increase the relative proportion of the hematite fraction and possibly the MD magnetite that has resisted dissolution, which explains the marked coarsening observed below this fine-grained interval. This transformation would be favoured by progressive depletion of Fe^{2+} with depth, which allows enough build-up of HS^- to produce elemental sulphur (S^0) (Pyzik and Sommer, 1981; Yao and Millero, 1996; Poulton et al., 2004), which is considered necessary for the final transformation of greigite into pyrite (Sweeney and Kaplan, 1973; Benning et al., 2000).

Greigite precipitation driven by interaction of reactive Fe with the HS^- produced by sulphate reduction during anaerobic oxidation of methane (Neretin et al., 2004; Garming et al., 2005; Larrasoaña et al., 2007; Van Dongen et al., 2007) is the likely cause of the observed increase in $MIRM/TiO_2$ near the methanogenic zone (Fig. 5). Greigite is preserved at these depths due to low sulphate concentrations, which prevent HS^- build-up and formation of the S^0 necessary to proceed to complete pyritization. Greigite preservation under anoxic conditions has important implications in the fossil record, both as a marker of methane oxidation processes (Larrasoaña et al., 2007) as well as for carrying secondary remagnetizations that may compromise the paleomagnetic record (Roberts and Weaver, 2005; Rowan et al., 2009). However, if significant greigite formation occurs shortly after deposition and a stable magnetization is acquired, it can faithfully record the magnetic field and provide important paleomagnetic and magnetostratigraphic information (e.g. Vasiliev et al., 2007, 2008; Hüsing et al., 2009). Whether greigite is a complication or a carrier of information needs to be assessed on a case by case basis.

In zone C, the dominant anoxic conditions finally dissolve a significant fraction of the remaining reduction-resistant high-coercivity material. This is illustrated by the continuous decrease in HIRM and B_{cr} observed in core CGPL-00-6 and core ZV-1 (Figs. 4 and 7). Under sulphidic conditions and due to low concentrations of reactive Fe, greigite or pyrite can precipitate in association with Fe-rich phyllosilicates (Canfield et al., 1992; Jiang et al., 2001; Roberts and Weaver, 2005). High Fe/S ratios in SEM microprobe analyses positively confirm the occurrence of greigite in core CGPL-00-6 (Fig. 9f), which also explains the decreasing B_{cr} trend from maxima of ~100 mT to 50–60 mT at the bottom of zone C because greigite has a lower B_{cr} than hematite. With increasing anoxic conditions down-core, a decrease in the rate of greigite precipitation due to enhanced pyritization may also contribute to the observed B_{cr} decrease.

5.3. Temporal and spatial scales of early diagenetic processes

The rate of magnetite dissolution can be estimated by determining its half-life, which is the time necessary to reduce the magnetite concentration (χ, $IRM_{900\,mT}$ and ARM) to half its maximum value (Canfield et al., 1992; Emiroğlu et al., 2004). This approach can be applied to our sediments based on the predominance of magnetite in zone A and the relatively stable detrital contribution in this zone (Fig. 2). As expected, the outer ria (CGPL-00-6) has the slowest dissolution rates, with half-lives of 860 years based on the χ record, 900 years based on $IRM_{900\,mT}$, and 920 years based on ARM. The ARM-based half-lives must be regarded as an upper limit for magnetite dissolution because the greigite that is confined to microenvironments in this zone probably contribute to the measured ARM due to its typically SD behaviour (Roberts, 1995) and the preferential acquisition of ARM by SD particles (Maher, 1988). This greigite contribution will counteract the ARM loss due to magnetite dissolution. For core CGVIR-36, we considered a range of sedimentation rates from 50 cm/kyr for core CGPL-00-6 from the outer ria to 360 cm/kyr for core VIR-18 (Diz et al., 2002) from the middle ria. Magnetite half-lives for core CGVIR-36 calculated in this way are 55–400, 63–460 and 72–520 years based on χ, $IRM_{900\,mT}$ and ARM, respectively. For core ZV-1, magnetite half-lives drop to ~45 years, with no significant differences (<4 years) between χ, $IRM_{900\,mT}$ and ARM. Overall, these half-lives agree with the 50–1000 year range proposed by Canfield and Berner (1987) for Long Island Sound (USA). The clear trend of shorter magnetite half-lives toward the interior of the ria highlights the strong gradient in reducing conditions caused by increased continental influence and organic matter input toward the inner parts of the ria. On the contrary, delayed onset of anoxic conditions in the outer ria sediments is likely caused by wave-forced resuspension of sediments, which promotes more efficient oxidation of organic matter within the water column as reported for the same sector of the adjacent Ria de Pontevedra (Rey et al., 2005). This early diagenetic gradient is also reflected in the surficial distribution of magnetic susceptibility (Rey et al., 2000). Higher susceptibilities in the outer ria occur where the magnetite half-life is longer, which is indicative of a lower dissolution rate and therefore of a higher concentration of magnetite, whereas shorter magnetite half-lives in the inner ria are associated with low susceptibility values, caused by increasing rates of dissolution.

5.4. Implications for shallow water environments

Similar diagenetic zonations have been observed in other environmental magnetic studies of coastal environments, such as the adjacent Ria de Pontevedra (Rey et al., 2005) and Ria de Arousa (Emiroğlu et al., 2004), as well as the Korean continental shelf (Liu et al., 2004), the Okhotsk Sea (Kawamura et al., 2007) and offshore Oregon, New Zealand and the Oman Margin (Rowan et al., 2009). Liu et al. (2004) described a similar zonation in two post-middle Holocene cores with uniform lithology and geochemical properties. Their diagenetic zonation was slightly expanded compared to our cores. For example, the equivalent of their zone A extends down to 78 cm, compared to a maximum of 40 cm in this study. These differences probably arise from the lower organic carbon content in their cores, which varies between 0.6% and 0.7%, which is 2–10 times lower than in our cores. These authors also defined an additional zone at the bottom of the sequence that is dominated by greigite. Its origin was interpreted to result from arrested pyritization caused by high TOC and iron activity according to the mechanism proposed by Kao et al. (2004). Alternatively, this zone may be analogous to the lower part of cores CGPL-00-6 and ZV-1, where greigite occurs in association with phyllosilicates, and with the estimated position of the sulphate-methane transition as indicated by the presence of gas bubbles.

In reductive environments, magnetic mineral grain size usually increases during dissolution (e.g. Liu et al., 2004; Kawamura et al., 2007) because fine-grained minerals dissolve more rapidly than coarse-grained particles due to the higher surface area to volume ratio of smaller particles. However, our cores undergo a magnetic fining associated with greigite precipitation in zone B. The TOC content in our cores is similar or higher than in other environments where only coarsening occurs, and more intense reducing conditions suggest that greigite is less likely to be preserved. To explain the longer persistence of greigite in sediments of the Ria de Vigo, we propose that this is due to more effective remineralization of organic matter in the water column. The forcing mechanism was first described in the adjacent Ria de Pontevedra (Rey et al., 2005) and involves occasional sediment resuspension by waves. This process effectively increases the residence time of organic matter as water depth increases, allowing more efficient oxidation of the labile fraction of the organic matter in the water column. A large fraction of the easily degraded organic matter will therefore have already been remineralized when the sediment finally settles, leading to slower respiration of the remaining, probably more refractory, organic matter and thus to a delay in the onset of anoxic conditions compared to the middle and inner ria. This mechanism can also explain the deepening of the magnetic zonation toward open ocean conditions, which is similar to that observed in the Okhotsk Sea (Kawamura et al., 2007). However, in the Ria de Vigo this occurs on much shorter distances and in a more closed and coastal environment, and is probably related to the higher organic matter supply toward the interior of the ria, where TOC reaches ~8%, as opposed to maximum reported values of ~2.3% in the Okhotsk Sea (Kawamura et al., 2007).

5.5. Preservation of paleoenvironmental signals

Rapid magnetic mineral dissolution in the Ria de Vigo, especially in its middle and inner parts, poses a serious drawback for using magnetic properties as paleoenvironmental and paleomagnetic proxies, as has been reported for other reductive sedimentary settings (e.g. Bloemendal et al., 1988, 1992; Yamazaki et al., 2003; Roberts and Weaver, 2005; Rowan et al., 2009). On the other hand, preservation of diagenetic magnetic zonations in the fossil record provides strong evidence for the past occurrence of highly reducing conditions, with Mediterranean sapropels being a remarkable example (e.g. Van Santvoort et al., 1997; Passier et al., 2001; Larrasoaña et al., 2003, 2006). Furthermore, detection of a spatial gradient like the one described here could be used to identify estuarine and ria environments, and help to identify coastal transitional settings between the open ocean and continents.

The documented magnetic zonation, and its significance in terms of the redox state of the sediment, also has important implications for other proxies that may be compromised by early diagenesis. In particular, metabolic dissolution and reprecipitation of $CaCO_3$ is caused by changes in pH and alkalinity that are driven by the by-products of organic C respiration (e.g. Emerson et al., 1980; Martin and Sayles, 2006; Schulz and Zabel, 2006). For example, the increase in CO_2 produced by respiration will decrease alkalinity (Emerson et al., 1980) and lead to acidification of pore waters to a pH in the range 6.0–8.3 (Ben Yaakov, 1973), which may be enough to dissolve $CaCO_3$. However, it has been argued that this pH is much higher than would be expected with dissolved CO_2 concentrations in pore waters as high as 60 mmol kg^{-1}; $CaCO_3$ dissolution has been proposed as a buffer mechanism to maintain pH at those levels (Ben Yaakov, 1973; Jourabchi et al., 2008). In suboxic and anoxic zones, higher alkalinity favours $CaCO_3$ preservation, while HS^- production causes dissolution unless it is buffered by pyritization in Fe-rich sediments (Schulz and Zabel, 2006). Therefore, care should be taken when interpreting proxies based on $CaCO_3$ or other components sensitive to the pH, alkalinity and/or redox changes associated with early diagenesis. Slower diagenesis in the outer ria can promote oxic dissolution of $CaCO_3$. In the middle and inner ria, shorter half-lives indicate faster onset of suboxic/anoxic conditions which favour $CaCO_3$ preservation. Observation of extensive Fe replacement in biogenic carbonates in sediments of the Galician rias (Rey et al., 2000, 2005) undergoing dissolution of magnetic minerals suggests potential alteration of the carbonate isotopic and elemental composition, which may bias interpretation of proxies such as Mg/Ca or Sr/Ca and even $\delta^{13}C$ and $\delta^{18}O$ (McCorkle et al., 1995; Hover et al., 2001; Rudnicki et al., 2001; Regenberg et al., 2006).

The clear diagenetic magnetic zonation developed in the Ria de Vigo demonstrates that magnetic properties are a sensitive tool for rapidly identifying problematic areas which can then be targeted with more elaborate and time-consuming techniques such as SEM or Laser Ablation ICP-MS analysis (Hathorne et al., 2003; Regenberg et al., 2007) for assessment of $CaCO_3$-based paleoceanographic proxies.

6. Conclusions

Early diagenesis is the main factor controlling the down-core evolution of magnetic properties of sediments from the Ria de Vigo, which produces a characteristic three-part zonation that can be traced along the outer, middle and inner sectors of the ria. Early diagenesis progresses more slowly in zones where water depth and sediment resuspension allow more efficient remineralization of organic matter in the water column. The result is a spatial trend in the diagenetic zonation, expressed as a deepening of the boundaries between the different magnetic zones.

Suboxic conditions prevail in the uppermost zone A, where the low degree of magnetic mineral dissolution does not significantly affect the magnetic properties. Sulphate reduction and pyrite and greigite authigenesis are confined to organic-rich microenvironments which also act as sinks for most of the Fe^{2+} produced in

this zone. Zone B is characterized by the almost complete dissolution of magnetic iron oxides. Elevated HS^- production caused by sulphate reduction explains the ubiquitous Fe-sulphide authigenesis. In the lower part of this zone, depletion of reactive Fe promotes transformation of greigite into pyrite. In zone C, the background magnetic signal is carried by hematite and probably MD magnetite that survived early diagenesis due to their slower rates of dissolution. In the lower part of zone C, remineralization of organic matter occurs mainly by methanogenesis, as indicated by the presence of gas bubbles. Greigite precipitation probably occurs as a by-product of anaerobic oxidation of methane in this zone.

Observation of similar diagenetic zonations in settings such as the adjacent Ria de Pontevedra and Ria de Arousa, the Korea Strait, the Okhotsk Sea, offshore Oregon, New Zealand and the Oman margin suggest that the studied processes are common in shallow marine environments with organic matter contents $>0.5\%$. In contrast, the magnetic fining associated with greigite precipitation at the beginning of the sulphidic/anoxic zone requires favourable conditions, which depend on factors such as TOC content, Fe availability and reactivity and sediment resuspension.

Magnetic properties have been successfully applied as a rapid, cost-effective and sensitive tool for detecting changes in sedimentary redox state. This has important implications for preservation of paleoenvironmental signals based on $CaCO_3$-related proxies. Therefore, preliminary magnetic screening can be valuable for identifying suitable sites for more detailed paleoenvironmental studies.

Acknowledgements

The research was supported by projects CTM2007-61227/MAR and PSS-310000-2006 from Spanish MICINN, PGDIT06-TAM3120PR and 09MMA012312PR of the Xunta de Galicia and IGCP-526 of the UNESCO. The authors would like to thank Dr. Alfonso. F. Davila for his assistance with the observation of magnetotactic bacteria and magnetosomes and his helpful comments on the manuscript. We are also grateful for comments from two anonymous reviewers. K.J. Mohamed acknowledges funding from the Spanish Ministry of Research, Science and Innovation/Fulbright Program and from a Marie Curie International Outgoing Fellowship within the 7th European Community Framework Programme.

References

Álvarez-Iglesias, P., Rubio, B., 2008. The degree of trace metal pyritization in subtidal sediments of a mariculture area: application to the assessment of toxic risk. Marine Pollution Bulletin 56, 973–983. doi:10.1016/j.marpolbul.2008.01.026.

Álvarez-Iglesias, P., Rubio, B., 2009. Redox status and heavy metal risk in intertidal sediments in NW Spain as inferred from the degrees of pyritization of iron and trace elements. Marine Pollution Bulletin 58, 542–551. doi:10.1016/j.marpolbul.2008.11.026.

Ben Yaakov, S., 1973. pH buffering of pore water of recent anoxic marine sediment. Limnology and Oceanography 18, 86–94.

Benning, L.G., Wilkin, R.T., Barnes, H.L., 2000. Reaction pathways in the Fe–S system below 100°C; direct observation and measurement of hydrothermal reactions. Chemical Geology 167, 25–51. doi:10.1016/S0009-2541(99)00198-9.

Berner, R.A., 1981. A new geochemical classification of sedimentary environments. Journal of Sedimentary Research 51, 359–365.

Blanchet, C.L., Thouveny, N., Vidal, L., 2009. Formation and preservation of greigite (Fe_3S_4) in sediments from the Santa Barbara Basin: implications for paleoenvironmental changes during the past 35 ka. Paleoceanography 24, PA2224. doi:10.1029/2008PA001719.

Bloemendal, J., Lamb, B., King, J., 1988. Paleoenvironmental implications of rock-magnetic properties of Late Quaternary sediment cores from the eastern equatorial Atlantic. Paleoceanography 3, 61–87.

Bloemendal, J., deMenocal, P., 1989. Evidence for a change in the periodicity of tropical climate cycles at 2.4 Myr from whole-core magnetic susceptibility measurements. Nature 342, 897–899. doi:10.1038/342897a0.

Bloemendal, J., King, J.W., Hall, F.R., Doh, S.-J., 1992. Rock magnetism of late Neogene and Pleistocene deep-sea sediments: relationship to sediment source, diagenetic processes, and sediment lithology. Journal of Geophysical Research 97, 4361–4375.

Bloemendal, J., King, J.W., Hunt, A., Demenocal, P.B., Hayashida, A., 1993. Origin of the sedimentary magnetic record at Ocean Drilling Program Sites on the Owen Ridge, western Arabian Sea. Journal of Geophysical Research 98, 4199–4219.

Blott, S.J., Pye, K., 2001. GRADISTAT: a grain size distribution and statistics package for the analysis of unconsolidated sediments. Earth Surface Processes and Landforms 26, 1237–1248. doi:10.1002/esp.261.

Caetano, M., Prego, R., Vale, C., de Pablo, H., Marmolejo-Rodríguez, J., 2009. Record of diagenesis of rare earth elements and other metals in a transitional sedimentary environment. Marine Chemistry 116, 36–46. doi:10.1016/j.marchem.2009.09.003.

Canfield, D.E., Berner, R.A., 1987. Dissolution and pyritization of magnetite in anoxic marine sediments. Geochimica et Cosmochimica Acta 51, 645–659. doi:10.1016/0016-7037(87)90076-7.

Canfield, D.E., Raiswell, R., Bottrell, S.H., 1992. The reactivity of sedimentary iron minerals toward sulphide. American Journal of Science 292, 659–683.

Chang, L., Roberts, A.P., Tang, Y., Rainford, B.D., Muxworthy, A.R., Chen, Q., 2008. Fundamental magnetic parameters from pure synthetic greigite (Fe_3S_4). Journal of Geophysical Research 113, B06104. doi:10.1029/2007JB005502.

Day, R., Fuller, M., Schmidt, V.A., 1977. Hysteresis properties of titanomagnetites: grain-size and compositional dependence. Physics of the Earth and Planetary Interiors 13, 260–267. doi:10.1016/0031-9201(77)90108-X.

Dekkers, M.J., Passier, H.F., Schoonen, M.A.A., 2000. Magnetic properties of hydrothermally synthesized greigite (Fe_3S_4)—II. High- and low-temperature characteristics. Geophysical Journal International 141, 809–819. doi:10.1046/j.1365-246x.2000.00129.x.

Desprat, S., Sánchez Goñi, M.F., Loutre, M., 2003. Revealing climatic variability of the last three millennia in northwestern Iberia using pollen influx data. Earth and Planetary Science Letters 213, 63–78. doi:10.1016/S0012-821X(03)00292-9.

Diz, P., Frances, G., Pelejero, C., Grimalt, J.O., Vilas, F., 2002. The last 3000 years in the Ria de Vigo (NW Iberian Margin): climatic and hydrographic signals. The Holocene 12, 459–468. doi:10.1191/0959683602hl550rp.

Dunlop, D.J., 2002. Theory and application of the Day plot (M_{rs}/M_s versus H_{cr}/H_c) 1. Theoretical curves and tests using titanomagnetite data. Journal of Geophysical Research 107 (B3), 2056. doi:10.1029/2001JB000486.

Emerson, S., Jahnke, R., Bender, M., Froelich, P., Klinkhammer, G., Bowser, C., Setlock, G., 1980. Early diagenesis in sediments from the eastern equatorial Pacific. I. Pore water nutrient and carbonate results. Earth and Planetary Science Letters 49, 57–80. doi:10.1016/0012-821X(80)90150-8.

Emiroğlu, S., Rey, D., Petersen, N., 2004. Magnetic properties of sediment in the Ria de Arousa (Spain): dissolution of iron oxides and formation of iron sulphides. Physics and Chemistry of the Earth 29, 947–959. doi:10.1016/j.pce.2004.03.012.

Evans, M.E., Heller, F., 2003. Environmental Magnetism: Principles and Applications of Enviromagnetics. Academic Press (Elsevier), New York.

Fraga, F., 1981. Upwelling off the Galician coast, Northwest Spain. In: Richards, F.A. (Ed.), Coastal Upwelling Series. American Geophysical Union, Washington, DC, pp. 176–182.

Froelich, P.N., Klinkhammer, G.P., Bender, M.L., Luedtke, N.A., Heath, G.R., Cullen, D., Dauphin, P., Hammond, D., Hartman, B., Maynard, V., 1979. Early oxidation of organic matter in pelagic sediments of the eastern equatorial Atlantic: suboxic diagenesis. Geochimica et Cosmochimica Acta 43, 1075–1090. doi:10.1016/0016-7037(79)90095-4.

Garming, J.F.L., Bleil, U., Riedinger, N., 2005. Alteration of magnetic mineralogy at the sulphate–methane transition: analysis of sediments from the Argentine continental slope. Physics of the Earth and Planetary Interiors 151, 290–308. doi:10.1016/j.pepi.2005.04.001.

Geiss, C.E., Banerjee, S.K., 1997. A multi-parameter rock magnetic record of the last glacial–interglacial paleoclimate from south-central Illinois, USA. Earth and Planetary Science Letters 152, 203–216. doi:10.1016/S0012-821X(97)00133-7.

Gingele, F.X., Zabel, M., Kasten, S., Bonn, W.J., Nürnberg, C.C., 1999. Biogenic barium as a proxy for paleoproductivity: methods and limitations of application. In: Fischer, G., Wefer, G. (Eds.), Use of Proxies in Paleoceanography: Examples from the South Atlantic. Springer-Verlag, Berlin Heidelberg, pp. 345–364.

Haese, R.R., 2000. The reactivity of iron. In: Schulz, H.D., Zabel, M. (Eds.), Marine Geochemistry. Springer, Berlin, pp. 233–262.

Hanzlik, M., Winklhofer, M., Petersen, N., 2002. Pulsed-field-remanence measurements on individual magnetotactic bacteria. Journal of Magnetism and Magnetic Materials 248, 258–267. doi:10.1016/S0304-8853(02)00353-0.

Hathorne, E.C., Alard, O., James, R.H., Rogers, N.W., 2003. Determination of intratest variability of trace elements in foraminifera by laser ablation inductively coupled plasma-mass spectrometry. Geochemistry, Geophysics, Geosystems 4, 8408. doi:10.1029/2003GC000539.

Horng, C.S., Torii, M., Shea, K.S., Kao, S.J., 1998. Inconsistent magnetic polarities between greigite- and pyrrhotite/magnetite-bearing marine sediments from the Tsailiaochi section, southwestern Taiwan. Earth and Planetary Science Letters 164, 467–481. doi:10.1016/S0012-821X(98)00239-8.

Hover, V.C., Walter, L.M., Peacor, D.R., 2001. Early marine diagenesis of biogenic aragonite and Mg-calcite; new constraints from high-resolution STEM and

AEM analyses of modern platform carbonates. Chemical Geology 175, 221–248. doi:10.1016/S0009-2541(00)00326-0.
Hüsing, S.K., Dekkers, M.J., Franke, C., Krijgsman, W., 2009. The Tortonian reference section at Monte dei Corvi (Italy): evidence for early remanence acquisition in greigite-bearing sediments. Geophysical Journal International 179, 125–143. doi:10.1111/j.1365-246X.2009.04301.x.
Hughen, K.A., Baillie, M.G.L., Bard, E., Bayliss, A., Beck, J.W., Bertrand, C.J.H., Blackwell, P.G., Buck, C.E., Burr, G.S., Cutler, K.B., Damon, P.E., Edwards, R.L., Fairbanks, R.G., Friedrich, M., Guilderson, T.P., Kromer, B., McCormac, F.G., Manning, S.W., Bronk Ramsey, C., Reimer, P.J., Reimer, R.W., Remmele, S., Southon, J.R., Stuiver, M., Talamo, S., Taylor, F.W., van der Plicht, J., Weyhenmeyer, C.E., 2004. Marine04 marine radiocarbon age calibration, 0–26 cal kyr BP. Radiocarbon 46, 1059–1086.
Jiang, W.-T., Horng, C.-S., Roberts, A.P., Peacor, D.R., 2001. Contradictory magnetic polarities in sediments and variable timing of neoformation of authigenic greigite. Earth and Planetary Science Letters 193, 1–12. doi:10.1016/S0012-821X(01)00497-6.
Jourabchi, P., Meile, C., Pasion, L.R., Van Cappellen, P., 2008. Quantitative interpretation of pore water O_2 and pH distributions in deep-sea sediments. Geochimica et Cosmochimica Acta 72, 1350–1364. doi:10.1016/j.gca.2007.12.012.
Kao, S.-J., Horng, C.-S., Roberts, A.P., Liu, K.-K., 2004. Carbon–sulfur–iron relationships in sedimentary rocks from southwestern Taiwan: influence of geochemical environment on greigite and pyrrhotite formation. Chemical Geology 203, 153–168. doi:10.1016/j.chemgeo.2003.09.007.
Karlin, R., Levi, S., 1983. Diagenesis of magnetic minerals in recent haemipelagic sediments. Nature 303, 327–330. doi:10.1038/303327a0.
Karlin, R., 1990. Magnetite diagenesis in marine sediments from the Oregon continental margin. Journal of Geophysical Research 95, 4405–4419.
Kasten, S., Jørgensen, B.B., 2000. Sulphate reduction in marine sediments. In: Schulz, H.D., Zabel, M. (Eds.), Marine Geochemistry. Springer, Berlin, pp. 263–282.
Kawamura, N., Oda, H., Ikehara, K., Yamazaki, T., Shioi, K., Taga, S., Hatakeyama, S., Torii, M., 2007. Diagenetic effect on magnetic properties of marine core sediments from the southern Okhotsk Sea. Earth, Planets, and Space 59, 83–93.
Krs, M., Novak, F., Krsova, M., Pruner, P., Kouklikova, L., Jansa, J., 1992. Magnetic properties and metastability of greigite-smythite mineralization in brown-coal basins of the Krusne hory Piedmont, Bohemia. Physics of the Earth and Planetary Interiors 70, 273–287. doi:10.1016/0031-9201(92)90194-Z.
Larrasoaña, J.C., Roberts, A.P., Stoner, J.S., Richter, C., Wehausen, R., 2003. A new proxy for bottom-water ventilation in the eastern Mediterranean based on diagenetically controlled magnetic properties of sapropel-bearing sediments. Palaeogeography, Palaeoclimatology, Palaeoecology 190, 221–242. doi:10.1016/S0031-0182(02)00607-7.
Larrasoaña, J.C., Roberts, A.P., Hayes, A., Wehausen, R., Rohling, E.J., 2006. Detecting missing beats in the Mediterranean climate rhythm from magnetic identification of oxidized sapropels (Ocean Drilling Program Leg 160). Physics of the Earth and Planetary Interiors 156, 283–293. doi:10.1016/j.pepi.2005.04.017.
Larrasoaña, J.C., Roberts, A.P., Musgrave, R.J., Grácia, E., Piñero, E., Vega, M., Martínez-Ruiz, F., 2007. Diagenetic formation of greigite and pyrrhotite in gas hydrate marine sedimentary systems. Earth and Planetary Science Letters 261, 350–366. doi:10.1016/j.epsl.2007.06.032.
Leslie, B.W., Lund, S.P., Hammond, D.E., 1990. Rock magnetic evidence for the dissolution and authigenic growth of magnetic minerals within anoxic marine sediments of the California continental borderland. Journal of Geophysical Research 95, 4437–4452.
Liu, J., Zhu, R., Roberts, A.P., Li, S., Chang, J.-H., 2004. High-resolution analysis of early diagenetic effects on magnetic minerals in post-middle-Holocene continental shelf sediments from the Korea Strait. Journal of Geophysical Research 109, B03103. doi:10.1029/2003JB002813.
Lyle, M., 1983. The brown–green color transition in marine sediments: a marker of the Fe(III)-Fe(II) redox boundary. Limnology & Oceanography 28, 1026–1033.
Maher, B.A., 1988. Magnetic properties of some synthetic sub-micron magnetites. Geophysical Journal of the Royal Astronomical Society 94, 83–96. doi:10.1111/j1365-246X.1988.tb03429.x.
Mann, S., Sparks, N.H.C., Frankel, R.B., Bazylinski, D.A., Jannasch, H.W., 1990. Biomineralization of ferrimagnetic greigite (Fe_3S_4) and iron pyrite (FeS_2) in a magnetotactic bacterium. Nature 343, 258–261. doi:10.1038/343258a0.
Martin, W.R., Sayles, F.L., 2006. Organic matter oxidation in deep-sea sediments: distribution in the sediment column and implications for calcite dissolution. Deep-Sea Research II 53, 771–792. doi:10.1016/j.dsr2.2006.01.017.
McCorkle, D.C., Martin, P.A., Lea, D.W., Klinkhammer, G.P., 1995. Evidence of a dissolution effect on benthic foraminiferal shell chemistry: $\delta^{13}C$, Cd/Ca, Ba/Ca, and Sr/Ca results from the Ontong Java Plateau. Paleoceanography 10, 699–714. doi:10.1029/95PA01427.
Moreno, E., Thouveny, N., Delanghe, D., McCave, I.N., Shackleton, N.J., 2002. Climatic and oceanographic changes in the Northeast Atlantic reflected by magnetic properties of sediments deposited on the Portuguese Margin during the last 340 ka. Earth and Planetary Science Letters 202, 465–480. doi:10.1016/S0012-821X(02)00787-2.
Munsell Color Company, 1994. Munsell Soil Color Charts. Revised Edition. Macbeth Division of Kollmorgen, New Windsor, NY.
Muñoz Sobrino, C., García-Gil, S., Diez, J.B., Iglesias, J., 2007. Palynological characterization of gassy sediments in the inner part of Ría de Vigo (NW Spain). New chronological and environmental data. Geo-Marine Letters 27, 289–302. doi:10.1007/s00367-007-0078-y.
Nagata, T., Carleton, B.J., 1987. Magnetic remanence coercivity of rocks. Journal of Geomagnetism and Geoelectricity 39, 447–461.
Neretin, L.N., Böttcher, M.E., Jørgensen, B.B., Volkov, I.I., Lüschen, H., Hilgenfeldt, K., 2004. Pyritization processes and greigite formation in the advancing sulfidization front in the upper Pleistocene sediments of the Black Sea. Geochimica et Cosmochimica Acta 68, 2081–2093. doi:10.1016/S0016-7037(03)00450-2.
Passier, H.F., de Lange, G.J., Dekkers, M.J., 2001. Magnetic properties and geochemistry of the active oxidation front and the youngest sapropels in the Mediterranean. Geophysical Journal International 145, 604–614.
Posfai, M., Cziner, K., Marton, E., Marton, P., Buseck, P.R., Frankel, R.R.B., Bazylinski, D.A., 2001. Crystal-size distributions and possible biogenic origin of Fe sulphides. European Journal of Mineralogy 13, 691–703. doi:10.1127/0935-1221/2001/0013-0691.
Poulton, S.W., Krom, M.D., Raiswell, R., 2004. A revised scheme for the reactivity of iron (oxyhydr)oxide minerals toward dissolved sulphide. Geochimica et Cosmochimica Acta 68, 3703–3715. doi:10.1016/j.gca.2004.03.012.
Prego, R., 1993. General aspects of carbon biogeochemistry in the Ria de Vigo, northwestern Spain. Geochimica et Cosmochimica Acta 57, 2041–2052. doi:10.1016/0016-7037(93)90092-B.
Pyzik, A.J., Sommer, S.E., 1981. Sedimentary iron monosulphides; kinetics and mechanism of formation. Geochimica et Cosmochimica Acta 45, 687–698. doi:10.1016/0016-7037(81)90042-9.
Regenberg, M., Nürnberg, D., Steph, S., Groenveld, J., Garbe-Schoenberg, D., Tiedemann, R., Dullo, W., 2006. Assessing the effect of dissolution on planktonic foraminiferal Mg/Ca ratios; evidence from Caribbean core tops. Geochemistry, Geophysics, Geosystems 7, Q07P15. doi:10.1029/2005GC001019.
Regenberg, M., Nürnberg, D., Schönfeld, J., Reichart, G.-J., 2007. Early diagenetic overprint in Caribbean sediment cores and its effect on the geochemical composition of planktonic foraminifera. Biogeosciences 4, 957–973. doi:10.5194/bgd-4-2179-2007.
Rey, D., López-Rodríguez, N., Rubio, B., Vilas, F., Mohamed, K., Pazos, O., Bógalo, M.F., 2000. Magnetic properties of estuarine-like sediments. The study case of the Galician Rias. Journal of Iberian Geology 26, 151–170.
Rey, D., Mohamed, K.J., Bernabeu, A., Rubio, B., Vilas, F., 2005. Early diagenesis of magnetic minerals in marine transitional environments: geochemical signatures of hydrodynamic forcing. Marine Geology 215, 215–236. doi:10.1016/j.margeo.2004.12.001.
Rey, D., Rubio, B., Mohamed, K., Vilas, F., Alonso, B., Ercilla, G., Rivas, T., 2008. Detrital and early diagenetic processes in Late Pleistocene and Holocene sediments from the SW Galicia Bank inferred from high-resolution enviromagnetic and geochemical records. Marine Geology 249, 64–92. doi:10.1016/j.margeo.2007.09.013.
Roberts, A.P., 1995. Magnetic properties of sedimentary greigite (Fe_3S_4). Earth and Planetary Science Letters 134, 227–236. doi:10.1016/0012-821X(95)00131-U.
Roberts, A.P., Pillans, B.J., 1993. Rock magnetism of Lower/Middle Pleistocene marine sediments, Wanganui Basin, New Zealand. Geophysical Research Letters 20, 839–842. doi:10.1029/93GL00802.
Roberts, A.P., Turner, G.M., 1993. Diagenetic formation of ferrimagnetic iron sulphide minerals in rapidly deposited marine sediments, South Island, New Zealand. Earth and Planetary Science Letters 134, 257–273. doi:10.1016/0012-821X(93)90226-Y.
Roberts, A.P., Weaver, R., 2005. Multiple mechanisms of remagnetization involving sedimentary greigite (Fe_3S_4). Earth and Planetary Science Letters 231, 263–277. doi:10.1016/j.epsl.2004.11.024.
Robinson, S.G., 1986. The late Pleistocene palaeoclimatic record of North Atlantic deep-sea sediments revealed by mineral-magnetic measurements. Physics of the Earth and Planetary Interiors 42, 22–47. doi:10.1016/S0031-9201(86)80006-1.
Robinson, S.G., Sahota, J.T.S., 2000. Rock-magnetic characterization of early, redoxomorphic diagenesis in turbiditic sediments from the Madeira Abyssal Plain. Sedimentology 47, 367–394. doi:10.1046/j.1365-3091.2000.00298.x.
Robinson, S.G., Sahota, J.T.S., Oldfield, F., 2000. Early diagenesis in North Atlantic abyssal plain sediments characterized by rock-magnetic and geochemical indices. Marine Geology 163, 77–107. doi:10.1016/S0025-3227(99)00108-5.
Rousse, S., Kissel, C., Laj, C., Eiríksson, J., Knudsen, K.-L., 2006. Holocene centennial to millennial-scale climatic variability: evidence from high-resolution magnetic analyses of the last 10 cal kyr off North Iceland (core MD99-2275). Earth and Planetary Science Letters 242, 390–405. doi:10.1016/j.epsl.2005.07.030.
Rowan, C.J., Roberts, A.P., Broadbent, T., 2009. Reductive diagenesis, magnetite dissolution, greigite growth and paleomagnetic smoothing in marine sediments: a new view. Earth and Planetary Science Letters 277, 223–235. doi:10.1016/j.epsl.2008.10.016.
Rudnicki, M.D., Wilson, P.A., Anderson, W.T., 2001. Numerical models of diagenesis, sediment properties, and pore fluid chemistry on a paleoceanographic transect; Blake Nose, Ocean Drilling Program Leg 171B. Paleoceanography 16, 563–575. doi:10.1029/2000PA000551.
Sagnotti, L., Winkler, A., 1999. Rock magnetism and palaeomagnetism of greigite-bearing mudstones in the Italian peninsula. Earth and Planetary Science Letters 165, 67–80. doi:10.1016/S0012-821X(98)00248-9.
Sagnotti, L., Roberts, A.P., Weaver, R., Verosub, K.L., Florindo, F., Pike, C.R., Clayton, T., Wilson, G.S., 2005. Apparent magnetic polarity reversals due to remagnetization resulting from late diagenetic growth of greigite from siderite.

Geophysical Journal International 160, 89–100. doi:10.1111/j.1365-246X.2005.02485.x.
Schulz, H.D., Zabel, M., 2006. Marine Geochemistry. Springer, Berlin.
Simmons, S.L., Sievert, S.M., Frankel, R.B., Bazylinski, D.A., Edwards, K.J., 2004. Spatiotemporal distribution of marine magnetotactic bacteria in a seasonally stratified coastal salt pond. Applied Environmental Microbiology 70, 6230–6239. doi:10.1128/AEM.70.10.6230-6239.2004.
Skinner, B.J., Erd, R.C., Grimaldi, F.S., 1964. Greigite, the thio-spinel of iron: a new mineral. American Mineralogist 49, 543–555.
Snowball, I.F., 1991. Magnetic hysteresis properties of greigite (Fe_3S_4) and a new occurrence in Holocene sediments from Swedish Lappland. Physics of the Earth and Planetary Interiors 68, 32–40. doi:10.1016/0031-9201(91)90004-2.
Snowball, I., Moros, M., 2003. Saw-tooth pattern of North Atlantic current speed during Dansgaard–Oeschger cycles revealed by the magnetic grain size of Reykjanes Ridge sediments at 59°N. Paleoceanography 18, 1026. doi:10.1029/2001PA000732.
Soares, A.M.M., 1993. The ^{14}C content of marine shells: evidence for variability in coastal upwelling off Portugal during the Holocene. Isotope Techniques in the Study of Past and Current Environmental Changes in the Hydrosphere and the Atmosphere. International Atomic Energy Agency, Vienna, pp. 471–485.
Steinberger, B., Petersen, N., Petermann, H., Weiss, D.G., 1994. Movement of magnetic bacteria in time-varying magnetic fields. Journal of Fluid Mechanics 273, 189–211. doi:10.1017/S0022112094001904.
Stolz, J.F., 1993. Magnetosomes. Journal of General Microbiology 139, 1663–1670.
Strechie, C., André, F., Jelinowska, A., Tucholka, P., Guichard, F., Lericolais, G., Panin, N., 2002. Magnetic minerals as indicators of major environmental change in Holocene Black Sea sediments: preliminary results. Physics and Chemistry of the Earth 27, 1363–1370. doi:10.1016/S1474-7065(02)00119-5.
Stuiver, M., Reimer, P.J., 1993. Extended ^{14}C data base and revised CALIB 3.0 ^{14}C age calibration program. Radiocarbon 35, 215–230.
Sweeney, R.E., Kaplan, I.R., 1973. Pyrite framboid formation; laboratory synthesis and marine sediments. Economic Geology 68, 618–634. doi:10.2113/gsecongeo.68.5.618.
Tarduno, J.A., 1995. Superparamagnetism and reduction diagenesis in pelagic sediments – enhancement or depletion? Geophysical Research Letters 22 1337–1340. doi:10.1029/95GL00888.
Thompson, R., Oldfield, F., 1986. Environmental Magnetism. Allen & Unwin, London.
Van Dongen, B.E., Roberts, A.P., Schouten, S., Jiang, W., Florindo, F., Pancost, R.D., 2007. Formation of iron sulphide nodules during anaerobic oxidation of methane. Geochimica et Cosmochimica Acta 71, 5155–5167. doi:10.1016/j.gca.2007.08.019.
Van Santvoort, P.J.M., deLange, G.J., Langereis, C.G., Dekkers, M.J., Paterne, M., 1997. Geochemical and paleomagnetic evidence for the occurrence of "missing" sapropels in eastern Mediterranean sediments. Paleoceanography 12, 773–786.
Vasiliev, I., Dekkers, M.J., Krijgsman, W., Franke, C., Langereis, C.G., Mullender, T.A.T., 2007. Early diagenetic greigite as a recorder of the palaeomagnetic signal in Miocene–Pliocene sedimentary rocks of the Carpathian foredeep (Romania). Geophysical Journal International 171, 613–629. doi:10.1111/j.1365-246X.2007.03560.x.
Vasiliev, I., Franke, C., Meeldijk, J.D., Dekkers, M.J., Langereis, C.G., Krijgsman, W., 2008. Putative greigite magnetofossils from the Pliocene epoch. Nature Geoscience 1, 782–786. doi:10.1038/ngeo335.
Vilas, F., Nombela, M.A., García-Gil, E., García-Gil, S., Alejo, I., Rubio, B., Pazos, O., 1995. Cartografía de Sedimentos Submarinos: La Ría De Vigo. Escala 1:50.000 (Memoria y Mapas) Consellería de Pesca. Marisqueo e Acuicultura. Xunta de Galicia, Santiago de Compostela.
Vilas, F., Bernabeu, A.M., Méndez, G., 2005. Sediment distribution pattern in the Rias Baixas (NW Spain): main facies and hydrodynamic dependence. Journal of Marine Systems 54, 261–276. doi:10.1016/j.jmarsys.2004.07.016.
Wasilewski, P.J., 1973. Magnetic hysteresis in natural materials. Earth and Planetary Science Letters 20, 67–72. doi:10.1016/0012-821X(73)90140-4.
Wollast, R., 1998. Evaluation and comparison of the global carbon cycle in the coastal zone and in the open ocean. In: Brink, K.H., Robinson, A.R. (Eds.), The Sea. Wiley, New York, pp. 213–252.
Yamazaki, T., Abdeldayem, A.L., Ikehara, K., 2003. Rock-magnetic changes with reduction diagenesis in Japan Sea sediments and preservation of geomagnetic secular variation in inclination during the last 30,000 years. Earth, Planets and Space 55, 327–340.
Yao, W., Millero, F.J., 1996. Oxidation of hydrogen sulphide by hydrous Fe(III) oxides in seawater. Marine Chemistry 52, 1–16. doi:10.1016/0304-4203(95)00072-0.
Zheng, Y., Kissel, C., Zheng, H.B., Laj, C., Wang, K., 2010. Sedimentation on the inner shelf of the East China Sea: magnetic properties, diagenesis and paleoclimate implications. Marine Geology 268, 34–42. doi:10.1016/j.margeo.2009.10.009.